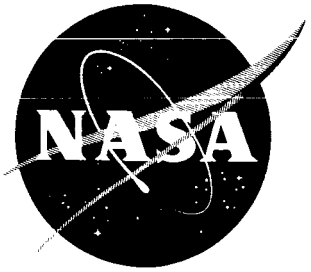

TECHNICAL MEMORANDUM
X-870

INTERSTAGE PRESSURES AND FORCES DURING HIGH-ALTITUDE STAGE SEPARATION WITH OPERATING UPPER-STAGE ENGINE

By Glenn A. Mitchell and Robert W. Cubbison

Lewis Research Center
Cleveland, Ohio

~~CLASSIFIED DOCUMENT~~ - TITLE UNCLASSIFIED

NATIONAL AERONAUTICS AND SPACE ADMINISTRATION
WASHINGTON
July 1963

NATIONAL AERONAUTICS AND SPACE ADMINISTRATION

TECHNICAL MEMORANDUM X-870

INTERSTAGE PRESSURES AND FORCES DURING HIGH-ALTITUDE STAGE SEPARATION WITH OPERATING UPPER-STAGE ENGINE*

By Glenn A. Mitchell and Robert W. Cubbison

SUMMARY

Pressure and forces that occur during stage separation were measured for various interstage and target configurations at a Mach number of 3.5 and pressure altitudes of 145,000 and 103,000 feet in the Lewis 10- by 10-foot supersonic wind tunnel. Air at chamber pressures up to 600 pounds per square inch absolute simulated the upper-stage-rocket exhaust. The sting-supported booster was translated to separation distances of 4.1 upper-stage diameters. Ratios of booster to upper-stage diameter were 1, 1.5, and 2. Dynamic booster releases from the strut-supported upper stage were also made.

At small separation distances, jet flow out of the interstage ports caused body boundary-layer flow separation over the entire upper stage. Misalinement of the booster under these conditions resulted in reasonably small upper-stage moments. Upper-stage-nozzle flow separation could also occur if the number and the open area of the interstage ports were inadequate when the booster was near the upper-stage base. Nozzle separation was symmetrical in all cases. The interstage-port area could be minimized without encountering nozzle flow separation by employing a large number of interstage ports rather than a small number. During the dynamic tests, no discernable moments were imparted to the booster or the upper stage.

INTRODUCTION

In order to maintain attitude control of the upper stage and to avoid liquid-propellant sloshing, upper-stage engine operation may be required before booster burnout and separation. The high-pressure hot exhaust gases would impose severe loads on the interstage hardware and the forward end of the lower-stage propellant tanks. Consequently, careful consideration must be given to the design of the interstage

*Title, Unclassified.

ports and the flow deflector (or target) within the interstage with the emphasis on minimizing the pressures and stage-interference effects. An understanding of the effect of port geometry and target shape on upper-stage nozzle flow, as well as on the pressures and forces affecting missile stability that are experienced by the separating stages, is necessary for a more rational approach to missile staging.

Previous work in the aerodynamics of missile staging (ref. 1) has been limited to low altitudes and low nozzle-pressure ratio and also to relatively few interstage configurations. An experimental investigation of the aerodynamic effects of different interstage configurations on missile-stage separation with the upper-stage rocket operating was made in the Lewis 10- by 10-foot supersonic wind tunnel at a free-stream Mach number of 3.5 and pressure altitudes of 145,000 and 103,000 feet. Both controlled and dynamic separations of the two stages were investigated.

SYMBOLS

A area

D drag

d upper-stage diameter

l distance upstream of upper-stage base

M Mach number

P total pressure

p static pressure

r radius

S recess distance (distance from target leading edge to interstage leading edge)

x separation distance (distance from upper-stage base to booster or interstage leading edge)

Subscripts:

a upper-stage afterbody

B booster

b base

c nozzle chamber

e nozzle exit

n nozzle wall

p interstage port

t target

0 free stream

Superscript:

* nozzle throat

APPARATUS AND PROCEDURE

The interstage configurations used in this investigation were designed to encompass the range of practical geometries for large vehicles. Schematic drawings and instrumentation details of the test model are shown in figure 1, and the various interstage and target configurations are shown in figure 2. The upper stage was a strut-mounted, 56.28-inch-long, 5-inch-diameter body with a 10°-half-angle conical nose. A flexible rubber seal between the nozzle and the base prevented flow into the inner cavity of the upper stage. The booster, a 36-inch-long cylinder, was sting-mounted from a separate support system with provisions for translating it during the controlled separation tests. Three boosters having diameters of 1, 1.5, and 2 upper-stage diameters were investigated. The various interstage units provided the structural transition from the upper stage to the booster. The forward surfaces of the 1.5- and 2-diameter-ratio interstages were 30° half-angle truncated cones. With all the ported configurations (4, 8, and 12 ports), the target within the interstage was a blunt cone of 45° half-angle. Other configurations also shown in figure 2 are the solid (or nonported) and the open interstage. The size and the design of the interstage ports were based on unpublished experimental data, which indicated that the port trailing edge should be coincident with, rather than upstream of the target surface, for the most efficient venting of the jet flow. To determine the effect of port-area distribution on the amount of discharge area needed to ensure unseparated nozzle flow, 4-, 8-, and 12-port interstages were investigated. Reductions in port area and interstage length were made by moving the target forward inside the interstage.

The open-interstage configurations were investigated to determine the interstage performance of vehicles attached by relatively thin structural members. The interstage fairing or cover structure normally

used for stream protection is removed in this concept, thereby resulting in an interstage of minimum length with maximum available vent area. The cover-structure weight is eliminated, but aerodynamic buffeting may become a problem.

A photograph of the dynamic test model showing a 1.5-diameter-ratio booster attached to the upper stage is shown in figure 3(a). The four struts used in the dynamic tests of the open-interstage configuration are shown in figure 3(b). Separation of the boost stage in the dynamic portion of the test was accomplished by mechanically pulling the pin from the spring-loaded clamping ring.

Operation of the upper-stage engine was simulated with cold air pressurized to a maximum of 600 pounds per square inch absolute. A nozzle with an area ratio of 25 was employed. The contour of the bell-shaped nozzle (fig. 4) corresponded to that of an optimum thrust nozzle (ref. 2). The nozzle extended 0.088 upper-stage diameter beyond the base and had an exit- to base-diameter ratio of 0.8. An alternate nozzle, a truncated isentropic nozzle (ref. 3), was also used for a limited number of interstage configurations. This nozzle (see fig. 4) was designed to give uniform parallel exit flow at an area ratio of 46.7 and was cut off at an area ratio of 25. Additional design details are given in reference 4.

The upper stage was instrumented with static-pressure orifices on the base, afterbody surface, and (for force data reduction) inside the body opposite the strut opening. Two rows of static-pressure taps were installed diametrically opposite each other (top and bottom) on the internal surface of the nozzle. Forces on the shell excluding the nozzle were measured by a three-component, electric, strain gage balance. A similar balance system was used to measure the forces on the interstage and booster unit. Static-pressure orifices were located across the surface of the target. Upper-stage pitching moments were computed about the body midpoint, and moment coefficients were based on the body length and cross-sectional area. The absolute magnitude of the moment coefficients was limited in accuracy to ± 0.1; however, the relative accuracy between data points was ± 0.01.

During the dynamic portion of the test, upper-stage forces were recorded on oscillograph traces, and each separation was photographed by a high-speed motion-picture camera.

The investigation was conducted at a Mach number of 3.5 and a pressure altitude of approximately 145,000 feet with chamber pressures of 150, 300, and 600 pounds per square inch absolute. Limited data were also obtained at a Mach number of 3.5 at an altitude of 103,000 feet and in quiescent air at sea level. Controlled stage separation was accomplished by translating the sting-mounted booster over a range of

distance up to 4.1 upper-stage diameters with the jet in continuous operation. For the dynamic tests, a chamber pressure of 600 pounds per square inch absolute was employed.

RESULTS AND DISCUSSION

The data presented fall in two general categories: (1) steady-state pressure and force measurements obtained by controlled separation of the booster, and (2) transient data obtained during actual releases of the simulated booster from the upper stage. Unless otherwise stated, all data shown were obtained with the bell-shaped nozzle.

Controlled Separation Tests

Effects of upper-stage jet discharge on free-stream flow. - Most of the data were obtained at a pressure altitude of 145,000 feet. Limited data were taken at 103,000 feet to determine altitude effects and for better visual flow definition. This comparison is shown in the schlieren photographs (fig. 5) and by the upper-stage static-pressure distributions (fig. 6). With the booster close to the upper stage, the jet exhausting through the interstage ports induced severe boundary-layer separation on the upper stage. At the lower altitude, flow-angle measurements (fig. 5(a)) and afterbody static-pressure distributions (fig. 6(a)) indicated this separation extended about 4 upper-stage diameters forward of the base. As the booster was translated downstream, the point of flow separation moved off the body at some staging distance x/d between 0.2 and 0.8 (see second and third photographs of fig. 5(a) or static pressures of fig. 6(a)). As would be expected, the extent of this flow separation was reduced as nozzle chamber pressure was decreased. At a chamber pressure of 150 pounds per square inch absolute and $x/d = 0.2$, the leading edge of this region was downstream of the last static-pressure orifice (fig. 6(a)). The asymmetry apparent in the photographed separation cone of figure 5(a) was caused by the mounting-strut wake.

The region of boundary-layer separation on the upper stage was much more extensive at 145,000 feet than at the lower altitude. The flow separation was clearly defined within the area of the schlieren window at 103,000 feet (fig. 5(a)), while at the higher altitude this region extended beyond the area encompassed by the photographs (fig. 5(b)). Because of the low density, the separated region within the photographed area cannot be clearly seen. For close staging distances (photographs 1, 3, and 5 of fig. 5(b)) the flow separation engulfed the entire upper stage. The upper-stage afterbody static pressures at $x/d = 0.2$ (fig. 6(b)) increased with higher chamber pressures, which indicated that the shock cone angle enclosing the region of separated flow was steepening.

This can occur only if the separated region has moved forward to the tip of the body. Photographs 1 and 2 or 3 and 4 of figure 5(b) illustrate the rearward movement of the points of incipient separation with increased stage separation distance. At $x/d = 0.8$, the afterbody pressures indicated flow separation only at the maximum chamber pressure of 600 pounds per square inch absolute.

As a result of the upper stage being enclosed in a region of separated flow, large destabilizing moments were not encountered with the booster misalined behind the upper stage. Misalinement was accomplished by positioning the booster leading edge below the 0° angle-of-attack upper stage with the booster at 5° angle of attack. Under these conditions a misalinement of 0.4 upper-stage diameter at the minimum separation distance produced destabilizing moment coefficients on the upper stage of about 0.4. With both stages alined and at 5° angle of attack, a stabilizing moment coefficient of about 0.2 was obtained. Although there was considerable scatter in the measured moments, there did not appear to be any consistent variation with chamber pressure. When it was assumed that the upper stage of a vehicle, such as the Thor-Agena B, separated at the same Mach number and altitude as the test model and experienced a destabilizing moment coefficient of 0.4 upon separation, a rough calculation indicated that a motor gimbal angle of only 2° would counteract the induced moment.

Upper-stage base pressures. - The effect of interstage-port area on upper-stage base pressures is shown in figure 7(a). Data are presented for the 4-port interstage on a 1.5-diameter-ratio booster at the smallest stage separation distance tested (i.e., $x/d = 0.025$). Decreasing the port area from approximately five to two nozzle-exit areas produced a large increase in base pressure. With the port area held constant (a fixed-length interstage), increasing the number of ports from 4 to 12 (fig. 7(b)) reduced the base pressure. The slope of the curves indicate that still lower base pressure could be obtained by using more than 12 ports. Thus, an interstage of many ports separated by small webs or struts is better able to relieve the jet flow than one having the same port area distributed into a few ports with large webs, which the jet flow must negotiate. The trend of lower base pressure with more ports would not be expected to continue indefinitely because the port flow coefficient decreases as the port size decreases. The base pressure also varied considerably with the chamber pressure ratio; the largest increases occurred at the smallest port area.

The effect of port geometry on the base pressure diminished rapidly with increasing stage separation distance. This relation is illustrated in figure 8 with the 4-port interstage configurations in which the port-area ratio $A_p/A_e = 2.02$ and 5.01. These two configurations produced the maximum and minimum values of base pressure obtained with the ported type of interstage. The ratio of base pressure to free-stream static

pressure is presented as a function of separation distance for upper-stage rocket chamber pressures of 600 pounds per square inch absolute. The variation of base pressure with staging distance for the ported configurations was almost identical beyond $x/d = 0.8$. At x/d greater than 1.6, the base pressure was constant for all configurations except the flat target. The trends and levels obtained with the flat and blunt-cone target were expected to represent the extreme cases in terms of configuration effects on the base pressure. Measurements on all ported interstages showed base pressures that were between these extremes.

The effect of booster diameter on upper-stage base pressures is presented in figure 9 as a function of the stage separation distance. With jet-off staging (fig. 9(a)), base pressures, as expected, varied with booster diameter; the 2-diameter-ratio booster produced base pressure ratios approximately 0.7 above those obtained with the 1-diameter-ratio booster. With jet-on staging (fig. 9(b)), base-pressure levels are primarily affected for staging distances as large as 1.6 upper-stage diameters. The exact contribution of the booster diameter, however, cannot be determined from the figure because the interstage-port area, which greatly affects the base pressure, is different for each booster diameter.

Nozzle flow patterns. - Both nozzles used in this investigation had identical area ratios and wall angles at the nozzle exit (fig. 4) and were designed by techniques intended to provide isentropic flow. The bell nozzle, however, was about 15 percent shorter than the truncated isentropic nozzle and had a maximum wall expansion angle of 29.3° as compared with an angle of 23.1° for the longer nozzle. In two-dimensional wind tunnel nozzle design, the attainment of isentropic flow is limited by a maximum nozzle-wall angle of $1/2\ \nu_E$, where ν_E is the Prandtl-Meyer angle for the nozzle-exit Mach number (ref. 5). Overturning of the flow occurs if this angle is exceeded. Three-dimensionally, this maximum angle is not readily amenable to calculation and furthermore depends on the particular flow assumptions made. For example, when radial flow downstream of the nozzle throat (ref. 6) was assumed, the maximum angle ($1/4\ \nu_E$) was calculated to be 20.9° for the nozzles of this report. The schlieren photographs of the truncated isentropic nozzle with an expansion angle of 23.1° (fig. 10(a)), however, show essentially isentropic flow emanating from the nozzle. In the case of the bell nozzle, the maximum angle appears to have been exceeded because of the shock structure shown in the schlieren photograph of figure 10(b). The short isentropic nozzle of reference 7, with the identical contour of the bell nozzle of this report, produced similar shock patterns.

As illustrated in figure 10(c), the flow pattern of the bell nozzle was changed considerably when the booster was relatively close to the

upper stage. This pattern (observed with all booster configurations) was caused by target surface pressures of sufficient magnitude to feed forward into the low-energy jet core. Since this change in flow patterns was reflected in the booster pressures and forces, it appears that the nozzle type (or contour) can considerably affect the interstage flow characteristics during the staging sequence.

Effects of Configuration on Nozzle Flow

Separation of the upper-stage nozzle flow occurred for some of the interstage configurations with the booster close to the upper stage. Examples of the separation characteristics with the stages alined and at 0° angle of attack are shown in figure 11. Data are also shown for the booster being misalined 0.4 upper-stage diameter and at a 5° angle of attack relative to the upper stage. In all cases the nozzle flow separation was symmetrical. Also pressure oscillations measured near the nozzle-exit were less than 0.1 percent of the chamber pressure. Reducing the separation distance (in this case, the distance between the nozzle exit plane and the target leading edge) from $x/d = 0.39$ to 0.19 changed the nozzle flow from full flowing to separated flow at an area ratio of 8.

The effect of interstage-port area on the stage separation distance at which nozzle flow separation occurred is presented in figure 12(a). Data are shown for the 1.5-diameter-ratio booster with 4 ports, with no ports, and for the open-interstage, flat- and blunt-cone-target configurations. With a port-area ratio of 3.9 or greater, nozzle separation did not occur. As port area was reduced from 3.9 nozzle-exit areas, the nozzle remained separated out to progressively greater stage separation distances. With the port area reduced to 2 exit areas, the nozzle remained separated until the booster was translated downstream 0.17 upper-stage diameter; and with the nonported interstage, the nozzle remained separated until a distance of 0.42 upper-stage diameter was reached.

The importance of target shape on nozzle separation is illustrated by the curves for the open-interstage, flat- and blunt-cone-target configurations (fig. 12(a)). The flow areas for the two targets were assumed to be the annular areas from the nozzle-exit periphery perpendicular to the target. The flat target caused the nozzle to remain separated out to $x/d = 0.35$ while presenting a peripheral flow area to the nozzle of 1.32 nozzle-exit areas. With the leading edge of the blunt-cone target at the nozzle-exit plane, the nozzle flow did not separate although the flow area available was only 0.61 of the nozzle-exit area. This area, although much less than that of the various ported configurations, is much more efficient because the jet flow is not forced to negotiate large web structures in exiting from the interstage region. Thus, using only structural members of minimum cross-sectional area to

connect the upper stage to the blunt-cone-target booster allows minimizing the interstage length. Such an interstage was investigated during the dynamic portion of the test without any indication of nozzle flow separation although the flow area was slightly smaller than that of the controlled separation model due to the connecting structural members or struts.

A change in the distribution of the interstage-port area by increasing the number of ports also permitted the port area (and interstage length) to be reduced without inducing nozzle separation. For example, a 4-port configuration required a port area of 3.9 nozzle-exit areas to operate without nozzle separation at the minimum staging distance (fig. 12(b)), whereas with an 8-port configuration an area of only 2.02 nozzle-exit areas in a shorter interstage achieved the same results. The slope of the curves indicate that by adding more ports still smaller port areas could be used. Additional data presented in figure 12(b), obtained with the alternate (truncated isentropic) upper-stage nozzle, show that nozzle contour has a large effect on the amount of interstage-port area needed. As the data indicate, the alternate nozzle required more total port area for unseparated flow than the original nozzle did.

Interstage target pressures. - The pressure profiles obtained at various separation distances on a blunt-cone target within a 4-port interstage are presented in figure 13 for chamber pressures of 600, 300, and 150 pounds per square inch absolute. The shape of these profiles is typical of those obtained with all ported configurations. Because of the stagnating effect of the webs near the target periphery, the corresponding pressures were higher than those in the port plane. At separation distances less than $x/d = 0.8$, this peripheral pressure at the web was the highest pressure on the target, but at moderate distances (e.g., $x/d = 1.6$) the peak pressure occurred at the target center. This change in pressure distribution was associated with the change in flow described earlier. In general, the pressure ratio p_t/P_c was independent of chamber pressure.

Pressure profiles across the surface of the blunt-cone target with the open interstage are presented in figure 14. The asymmetry of the profiles was due to a slight misalinement of the booster. Target profiles (fig. 14(a)) were changed considerably when the alternate (truncated isentropic) nozzle was used in the upper stage (fig. 14(b)). This change did not significantly affect the level of booster drag or the peak target pressure obtained. The corresponding local heating rates on a target, however, may be affected by the change in pressure profiles.

Although the general shape of pressure profiles on the target was independent of port geometry, the pressure levels were not. This is shown in figure 15 where peak target pressures of profiles similar to

those of figure 13 are presented for variations of port-area ratio and distribution as a function of separation distance. The step change in the curves presented were again an effect of the previously mentioned nozzle-flow-pattern change. It was noted during the test that the nozzle flow pattern could change at any point over a short range of separation distances for any particular configuration. The location of the step changes shown were obtained by retracting the booster from the upper stage at a uniform speed. The highest level of target pressure occurred not at the minimum separation distance but immediately after the nozzle-flow-pattern change. These peaks (fig. 15(a)), an effect of nozzle contour and interstage geometry, were higher for the larger port areas (longer interstages). For port areas of approximately 4 to 5 nozzle-exit areas, maximum target pressures were about 18 percent of jet total pressure, while for port areas of about 2 to 3 exit areas, the pressures were approximately 6 percent. At the minimum separation distance, the largest port area tested (i.e., $A_p/A_e = 5.01$), produced the lowest peak pressure, $p_t/P_c = 0.039$. Decreasing the port area to 3.9 nozzle-exit areas increased the peak pressure at the minimum separation distance to 5.9 percent of chamber total pressure. Further decreases in port area had little effect at minimum separation distance.

Increasing the number of interstage ports (4, 8, to 12) while maintaining a constant port area (fig. 15(b)) decreased the peak target pressures both before and after the nozzle-flow-pattern change. At the minimum stage separation distance, this pressure was reduced from 5.6 to 3.8 percent of chamber total pressure as a result of the smaller flow stagnation regions produced by the narrower webs. Elimination of the web area, illustrated in figure 15(b) by the open-interstage configuration, reduced peak pressures before the shock change, whereas after the change they were about the same as those obtained for the 12-port configurations.

Booster drag. - Booster drag parameters for all configurations tested are presented in figure 16 as a function of stage separation distance. The step changes in the curves shown are a result of changes in target-pressure profiles produced by the two different nozzle flow patterns illustrated in figure 10. Where the data are presented as bands in figure 16, no consistent trend with configuration or chamber pressure was observed, and the step changes shown in these cases represent the limits between which the nozzle-flow-pattern changes occurred. The booster drags obtained for all ported interstage configurations tested with the 1.5-diameter-ratio booster (fig. 16(a)) were contained within a range starting at a drag parameter of 1.65 to 1.9 at $x/d = 0$ and decreasing to a range of 0.32 to 0.44 at a separation distance of 3.2 upper-stage diameters. The one exception, the 4-port interstage with a port area of 5.01 nozzle-exit areas, produced drag parameters initially about 0.5 lower than the other ported interstage configurations. After the nozzle-flow-pattern change, the drag for this configuration was

consistent with that produced by the other configurations. The booster drags obtained for ported interstage configurations with the alternate nozzle in the upper stage (data not presented) were essentially the same as the values obtained with the bell-shaped nozzle. The only difference was the absence of the step changes shown in figure 16.

The open-interstage, blunt-cone-target configurations had consistently lower drags than any other configuration except at a separation distance of 0.09 upper-stage diameter in the case of the 2-diameter-ratio booster (fig. 16(c)). In this instance, larger drag was obtained as a result of reducing the area available to the exiting jet flow to about one-half the nozzle-exit area.

The general level of the drag obtained with flat-target configurations increased with increasing booster diameter. For the 1.5- and 2-diameter-ratio boosters, the flat targets produced consistently higher drags than any other configuration. The minimum separation distance tested with the flat-target configuration was limited to that shown in figure 16 by nozzle separation.

One of the primary factors affecting the booster drag and also the upper-stage-base pressure was the shape of the target upon which the jet impinged. As shown in figure 17, the target shape determined the angle at which the jet flow was discharged from the interstage area. With the blunt-cone target (fig. 17(a)), the jet-flow discharge angle was somewhat greater than the cone angle of the target, which resulted in the smallest booster drag and upper-stage-base pressure measurements obtained (figs. 16 and 8). The addition to this target of an interstage with attendant interferences caused increases in both the booster drag and base pressure. The largest forces were obtained with the flat target because, as illustrated in figure 17(b), the jet flow was turned more than 90° and discharged from the interstage region in an upstream direction.

A variation in altitude from 145,000 to 103,000 feet (fig. 18) had little effect on the level of booster drag; the average difference in drag parameter was about 0.04 although the rocket pressure ratio varied from 860 to 4670 percent of design pressure ratio. Booster drag obtained in quiescent air at sea level was greatly different from the force obtained at the higher altitude; it was less than one-half the value at close stage separation distances. The nozzle pressure ratio at sea level was only 7.7 percent of design pressure ratio. Thus evaluations of interstage forces and pressures made from sea-level, quiescent-air data (with the nozzle overexpanded) would not be applicable at the altitude of actual staging.

Dynamic Tests

During the dynamic test phase, successful stage separation was achieved with all configurations. No destabilizing forces on the booster were discernable on any of the releases, and none were recorded on the upper stage. Selected frames from the high-speed film of one of the releases are shown in figure 19. The shock patterns observed from these photographs are the same as those obtained during the controlled separation tests. It was apparent from the films that all the released boosters moved downstream without pitch or vertical displacement. Cameras mounted in the vertical plane also showed no measurable yaw or lateral displacement. From timing marks on the photographic film and the grid lines on each photograph, it was possible to determine the separation rates of the booster.

Rates of separation were measured for two configurations: (1) a 12-port interstage and (2) a blunt-cone target with the minimum structural members (or struts) necessary to attach it to the upper stage. A photograph of the latter configuration, which except for the added struts was the same as the open-interstage, blunt-cone-target configuration of the controlled separation tests, is shown in figure 3(b). Rates of separation were also calculated from booster drag curves of the controlled separation tests and are compared with the measured rates in figure 20. Since good agreement was obtained from the calculated and measured separation rates, controlled separation tests can be used to determine the staging characteristics of vehicles.

SUMMARY OF RESULTS

Pressures and forces encountered during stage separation were investigated for various booster configurations over a range of separation distance. Tests were conducted at a Mach number of 3.5 and pressure altitudes of 145,000 and 103,000 feet. Cold air at chamber pressures up to 600 pounds per square inch absolute was used to simulate the upper-stage rocket exhaust. The following results were obtained:

1. With the upper-stage engine operating prior to staging, separated flow engulfed the entire upper stage at an altitude of 145,000 feet. At the lower altitude, the region of separated flow was less extensive.

2. As a result of this separated flow, no large moments were induced on the upper stage. With the upper stage at 0° angle of attack and the booster displaced 0.4 upper-stage diameters and separating at 5° angle of attack, the largest measured destabilizing moment was 0.4.

3. Large reductions of upper-stage base pressure were obtained by enlarging the interstage-port area. Also significant reductions were

obtained when the number of ports was increased from 4 to 12 while total port area remained constant.

4. Separation of flow inside the upper-stage nozzle could be induced by insufficient interstage-port area. In all instances, the nozzle separation was symmetrical.

5. With the requirement that the upper-stage engine operate without nozzle flow separation, increasing the number of interstage ports permitted the port area to be reduced with a concomitant decrease in interstage length. Complete removal of all interstage material except for thin connecting structural members resulted in an interstage of minimum length, in that operation was feasible with the target leading edge at the exit plane of the upper-stage nozzle.

6. Variations of port area and distribution did not significantly change the force experienced by the booster during jet-on staging.

7. The highest pressure on the target within an interstage were obtained for the larger port area interstages. Maximum target pressure did not occur at the minimum separation distance, but were associated with a change in the nozzle flow pattern.

8. No discernable moments were imparted to any of the boosters released during the dynamic tests. Good agreement was obtained between measured rates of separation and those calculated from force measurements of the controlled separation tests.

9. The nozzle type (or contour) used on the upper-stage engine had considerable effect on both the interstage flow and the nozzle flow-separation characteristics.

Lewis Research Center
National Aeronautics and Space Administration
Cleveland, Ohio, July 18, 1962

REFERENCES

1. Wasko, Robert A.: Experimental Investigation of Stage Separation Aerodynamics. NASA TN D-868, 1961.

2. Rao, G. V. R.: Exhaust Nozzle Contour for Optimum Thrust. Jet Prop., vol. 28, no. 6, June 1958, pp. 377-382.

3. Clippinger, R. F.: Supersonic Axially Symmetric Nozzles. Rep. 794, Ballistic Res. Lab., Aberdeen Proving Ground (Md.), Dec. 1951.

4. Farley, John M., and Campbell, Carl E.: Performance of Several Method-of-Characteristics Exhaust Nozzles. NASA TN D-293, 1960.

5. Kenney, J. T., and Webb, L. M.: A Summary of the Techniques of Variable Mach Number Supersonic Wind Tunnel Nozzle Design. AGARDograph 3, AGARD, Oct. 1954.

6. Landsbaum, Ellis M.: Contour Nozzles. Memo. 20-169, Jet Prop. Lab., C.I.T., Sept. 15, 1958.

7. Stitt, Leonard E.: Interaction of Highly Underexpanded Jets with Simulated Lunar Surfaces. NASA TN D-1095, 1961.

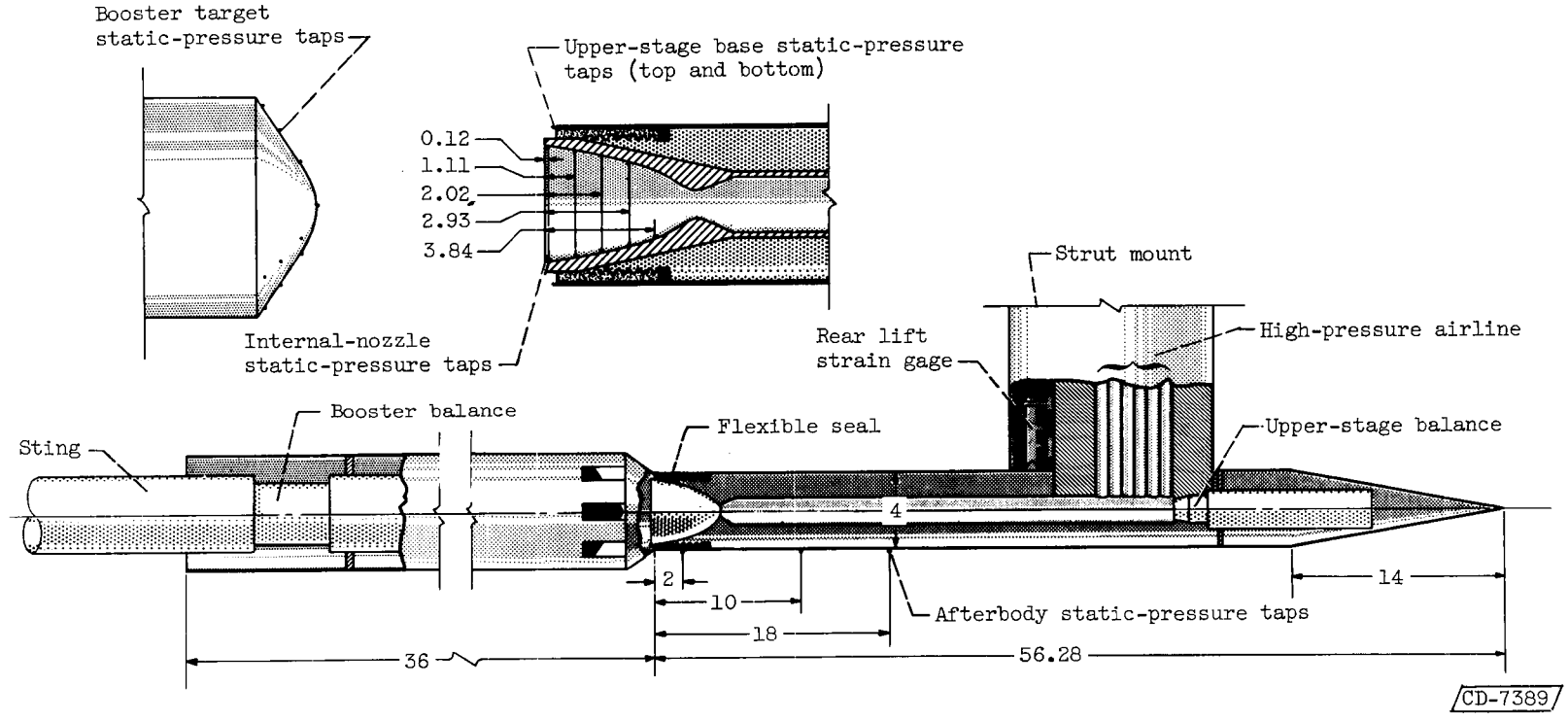

Figure 1. - Schematic diagram of upper-stage assembly and translatable 1.5-diameter-ratio booster.
(All dimensions in inches.)

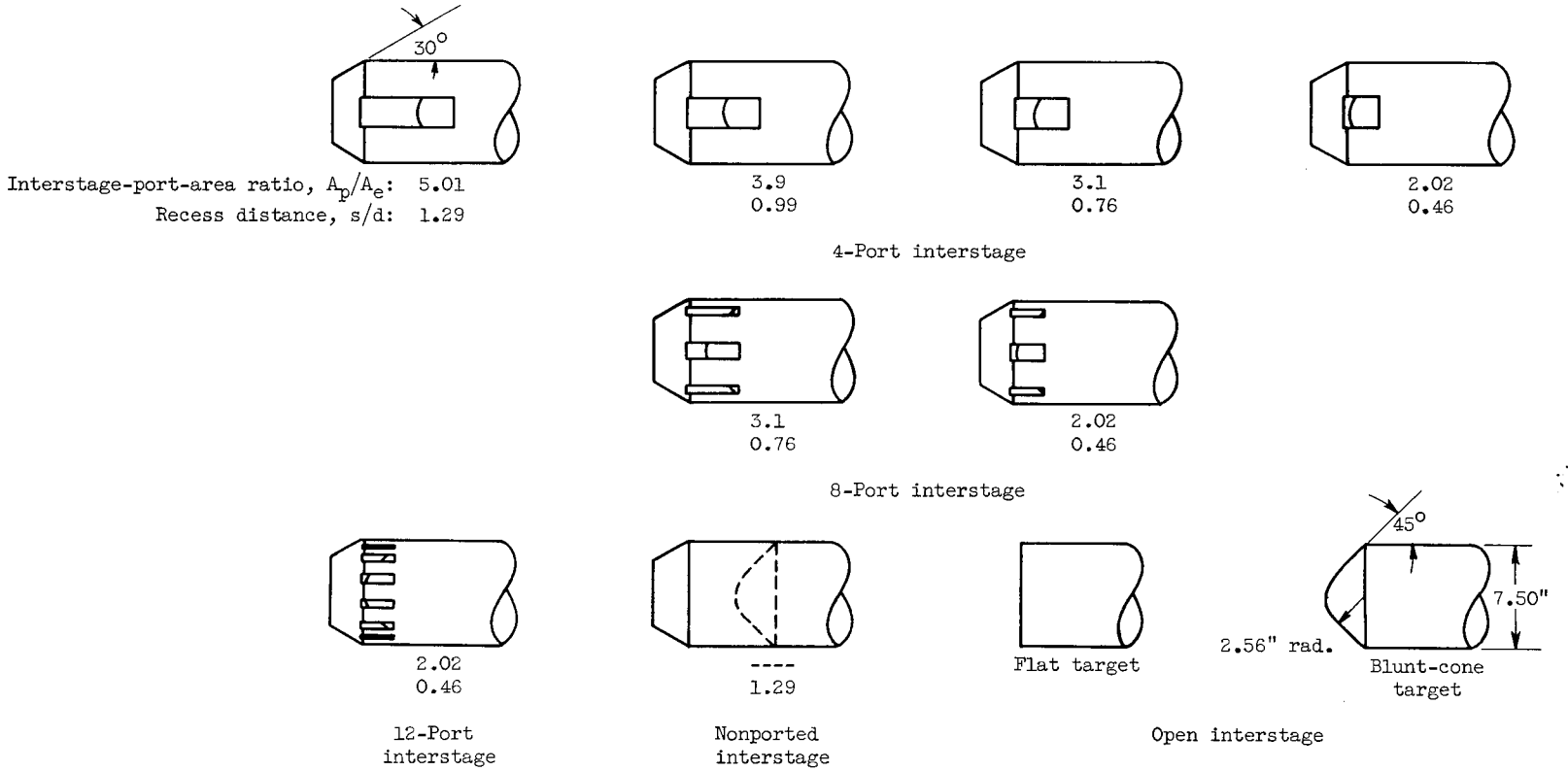

(a) 1.5-Diameter-ratio booster.

Figure 2. - Interstage and target configurations.

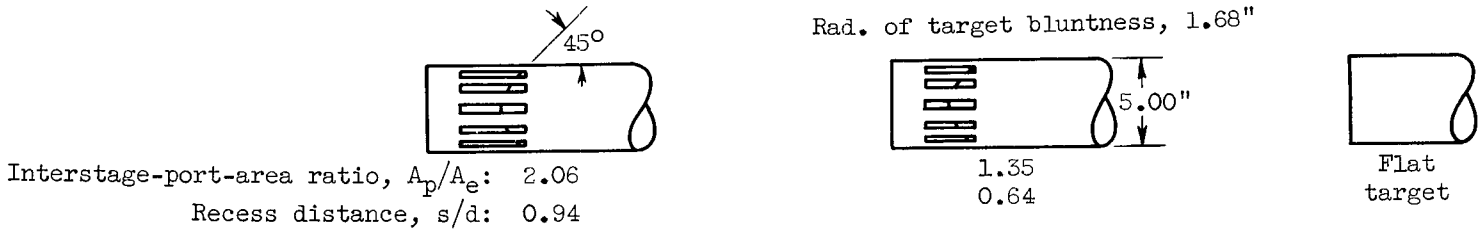

(b) 1-Diameter-ratio boosters.

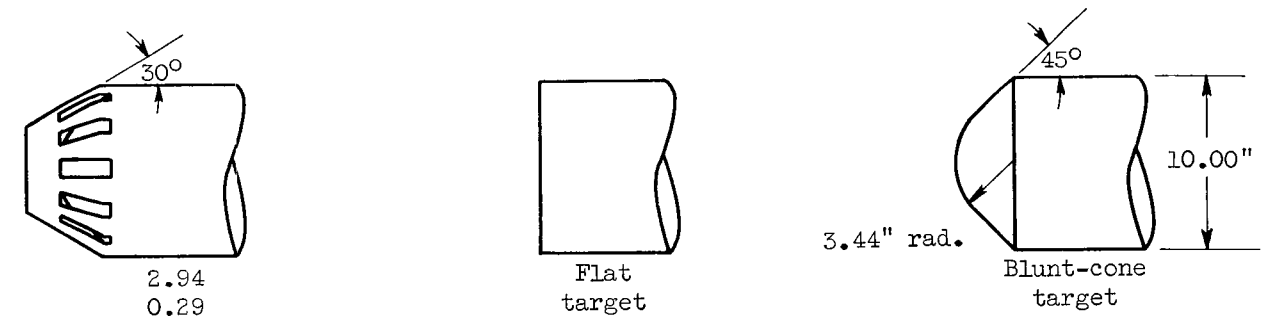

(c) 2-Diameter-ratio boosters.

Figure 2. - Concluded. Interstage and target configurations.

C-55832

(a) Strut-mounted upper stage with attached 1.5-diameter-ratio booster.

Figure 3. - Dynamic test model.

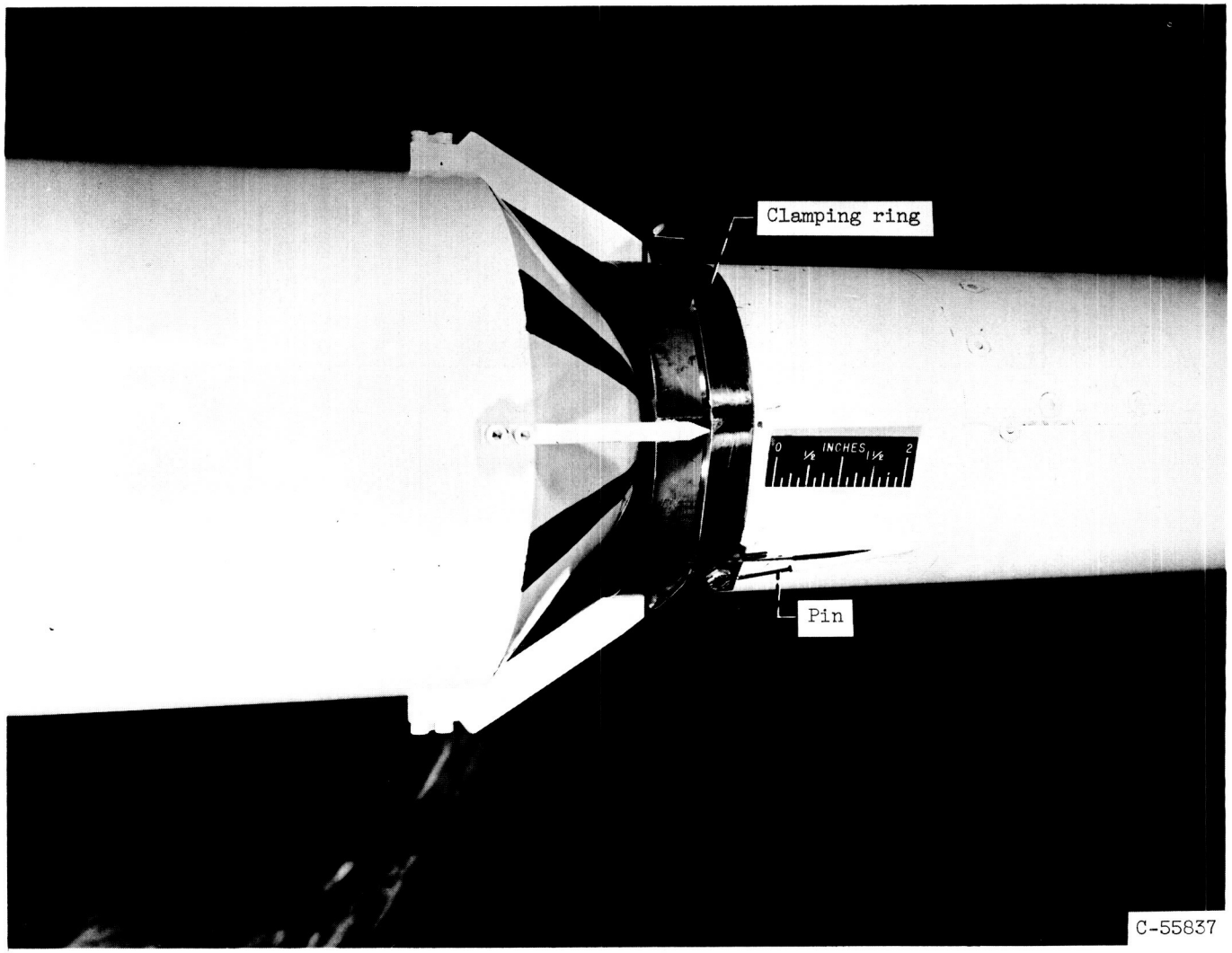

(b) 1.5-Diameter-ratio booster and open-interstage, blunt-cone-target configuration.

Figure 3. - Concluded. Dynamic test model.

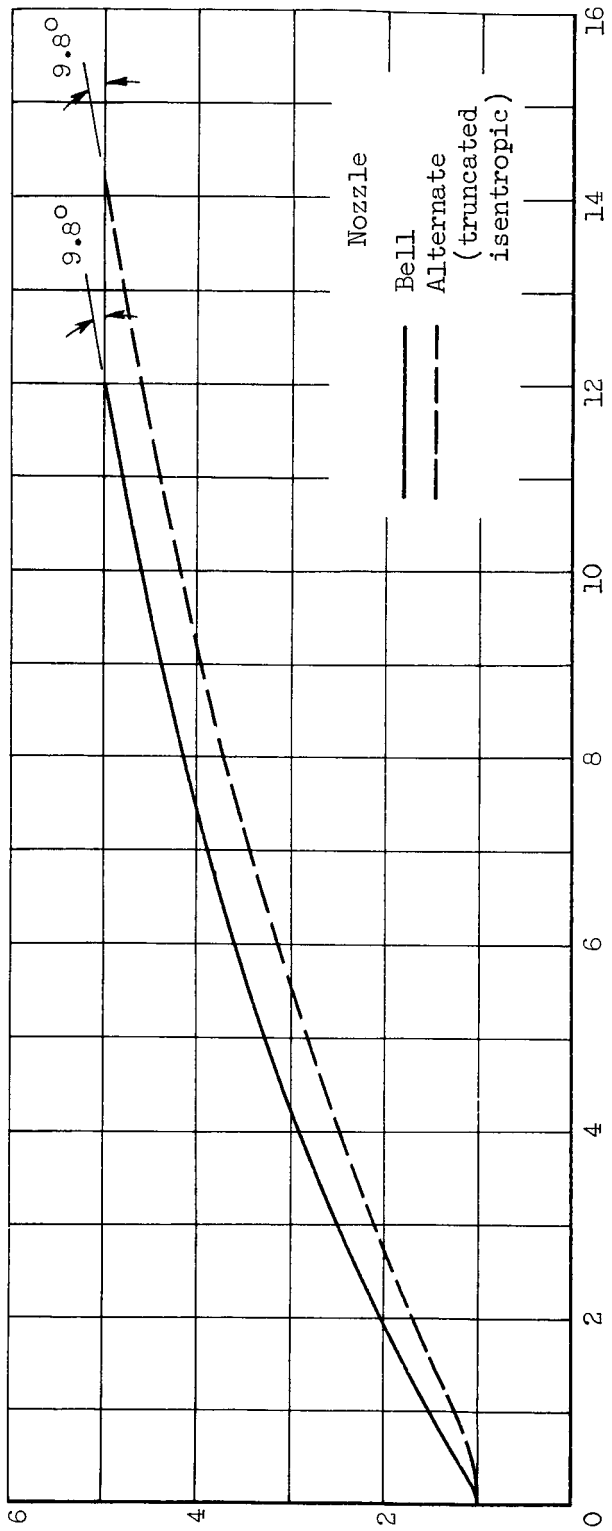

Figure 4. - Nozzle contours.

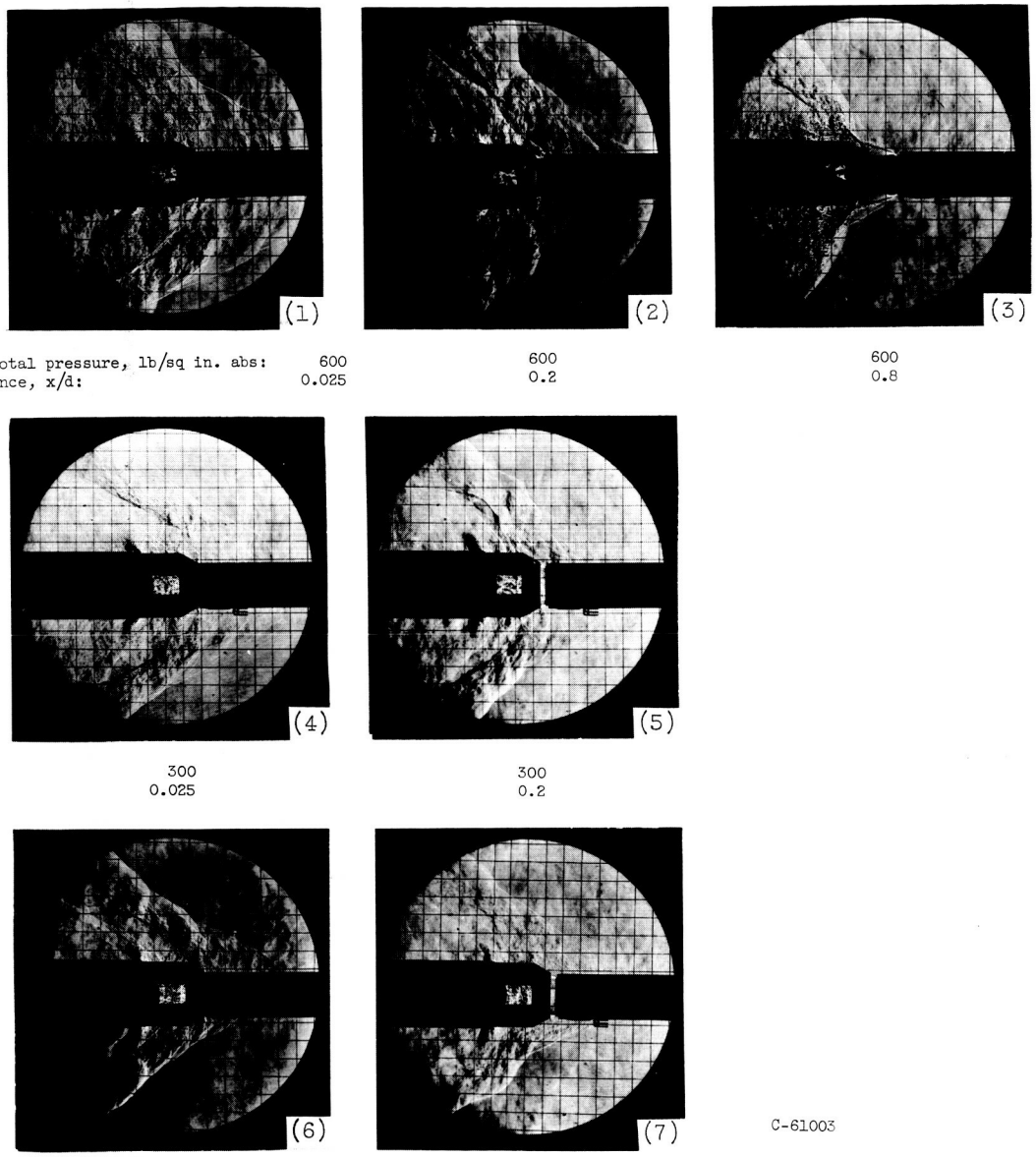

Nozzle-chamber total pressure, lb/sq in. abs:	600	600	600
Separation distance, x/d:	0.025	0.2	0.8
	300	300	
	0.025	0.2	
	150	150	
	0.025	0.2	

C-61003

(a) Altitude, 103,000 feet.

Figure 5. - Schlieren photographs of 1.5-diameter-ratio booster. Interstage-port-area ratio, 3.9.

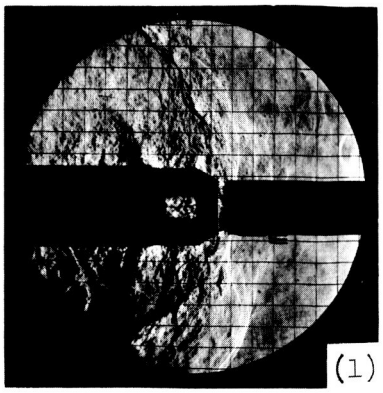

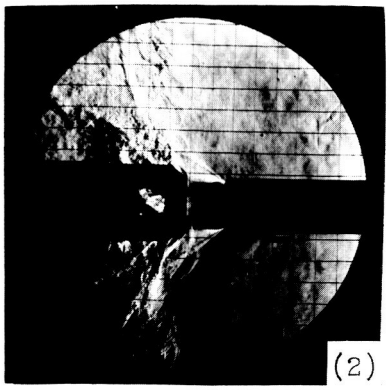

Nozzle-chamber total pressure, lb/sq in. abs:	600	600
Separation distance, x/d:	0.2	0.8

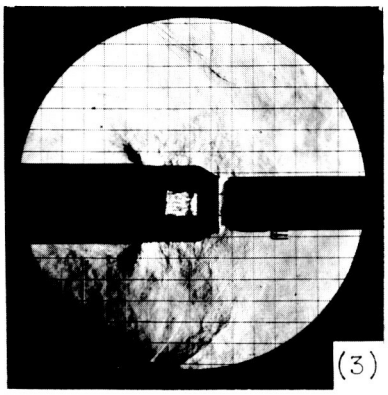

300	300
0.2	0.8

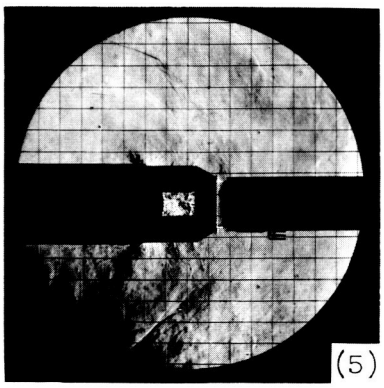

C-61004

150
0.2

(b) Altitude, 145,000 feet.

Figure 5. - Concluded. Schlieren photographs of 1.5-diameter-ratio booster. Interstage-port-area ratio, 3.9.

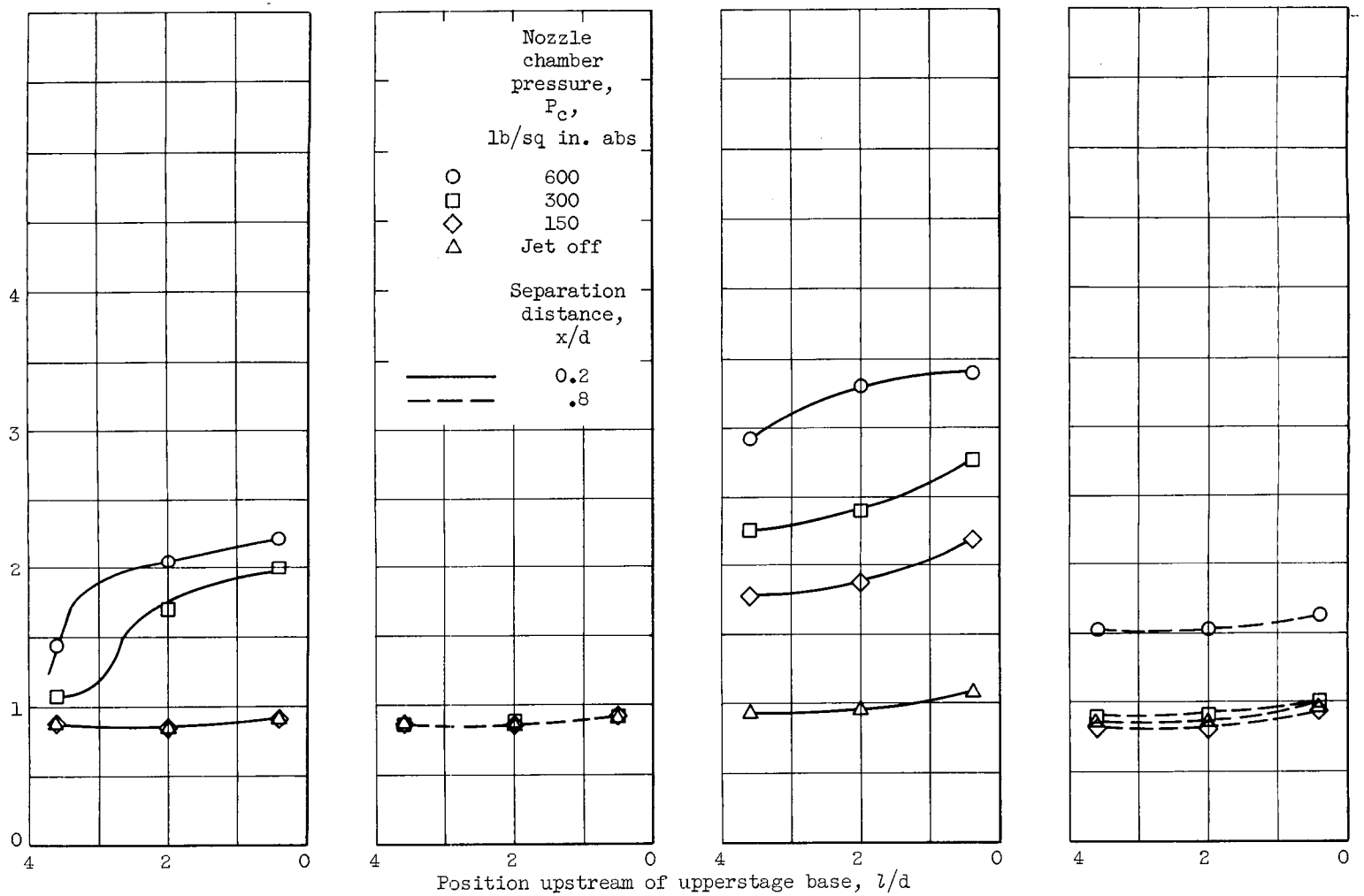

(a) Altitude, 103,000 feet.

(b) Altitude, 145,000 feet.

Figure 6. - Upper-stage afterbody pressure distributions. 1.5-Diameter-ratio booster; number of interstage ports, 4; interstage-port-area ratio, 3.9.

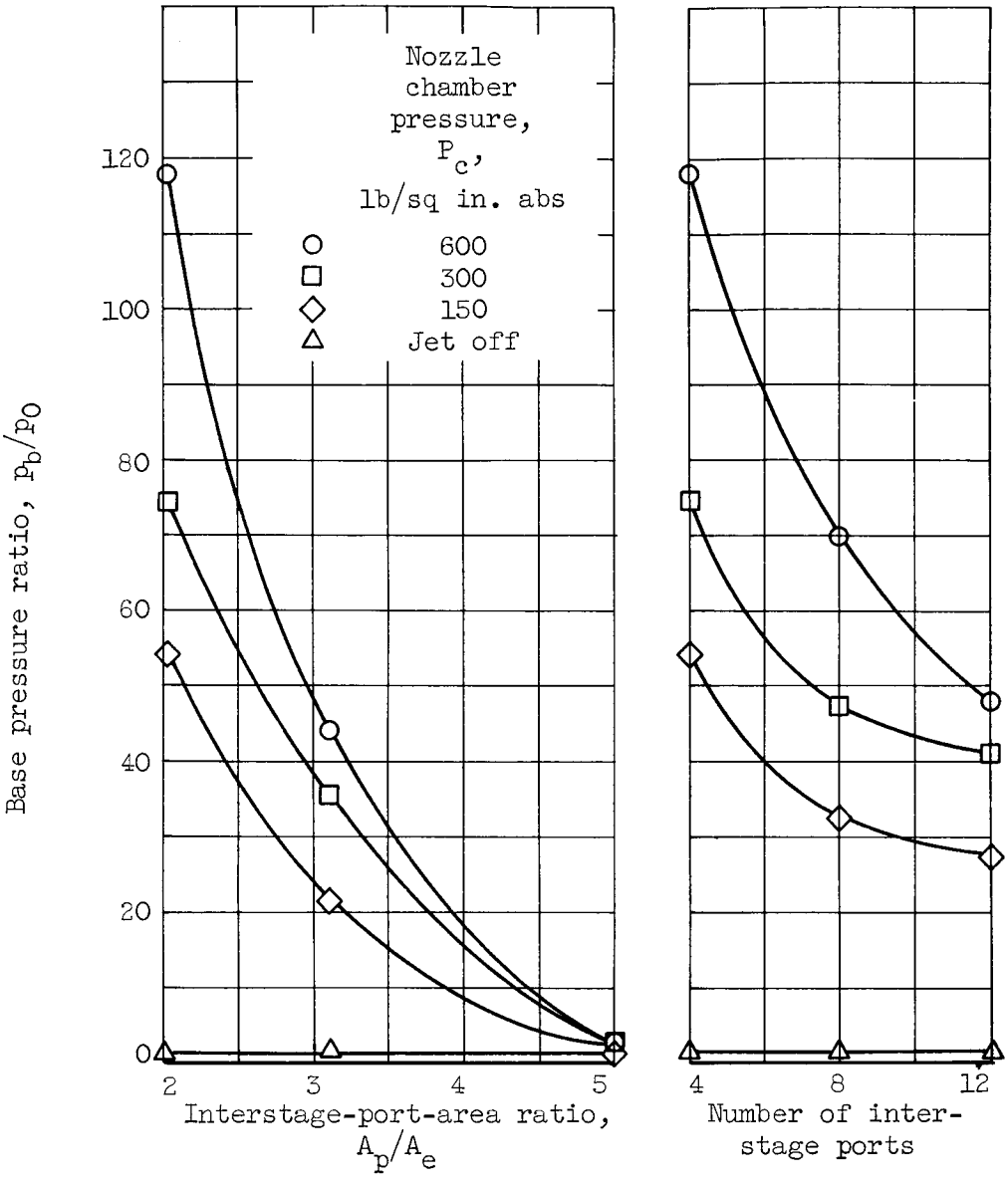

(a) Variation of port area. Number of interstage ports, 4.

(b) Variation of number of interstage ports. Interstage-port-area ratio, 2.02.

Figure 7. - Effect of interstage port configurations on upper-stage base pressure. 1.5-Diameter-ratio booster; separation distance, x/d = 0.025.

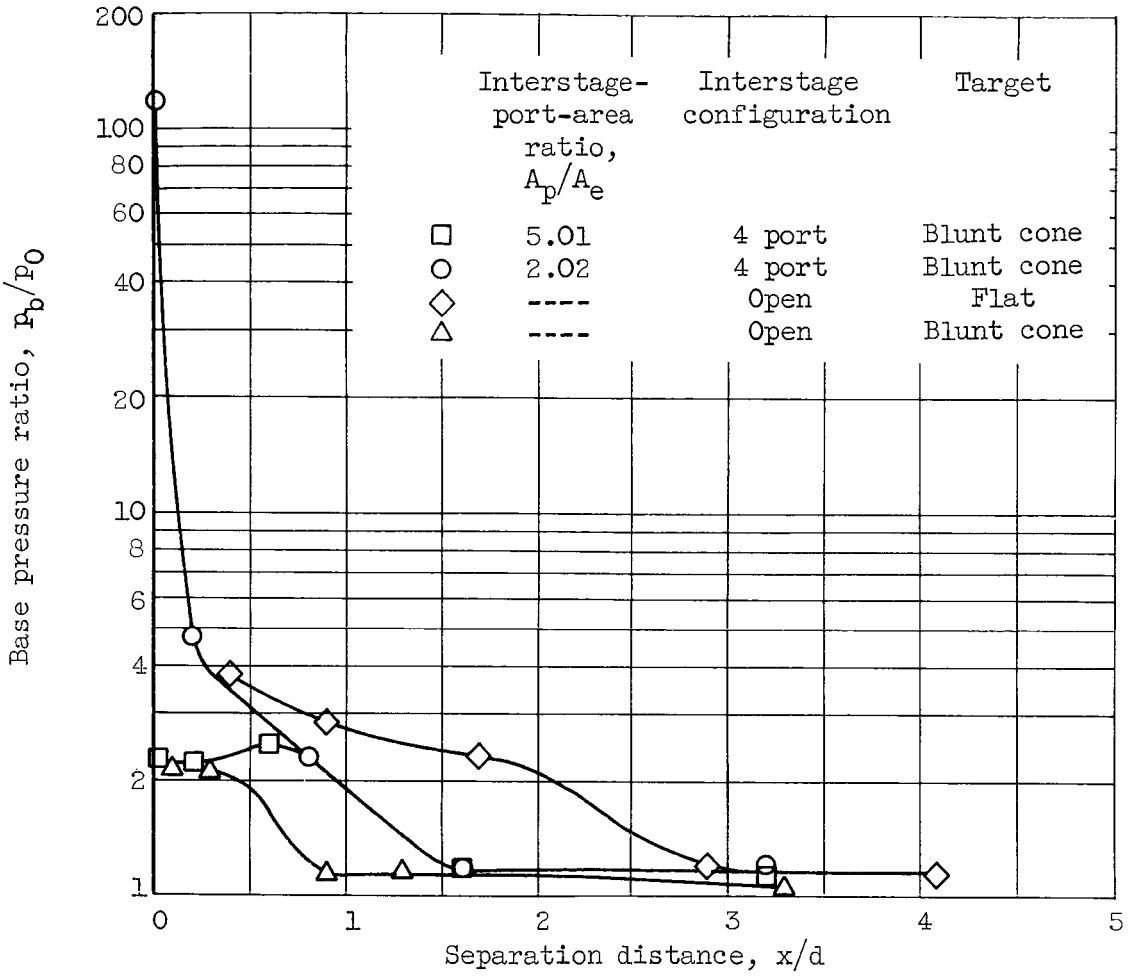

Figure 8. - Variation of upper-stage base pressure with separation distance. 1.5-Diameter-ratio booster; chamber pressure, 600 pounds per square inch absolute.

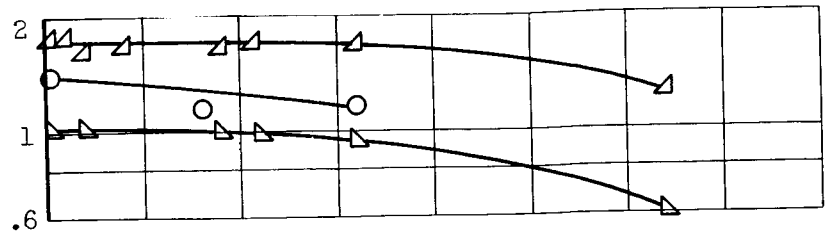

(a) Jet-off staging.

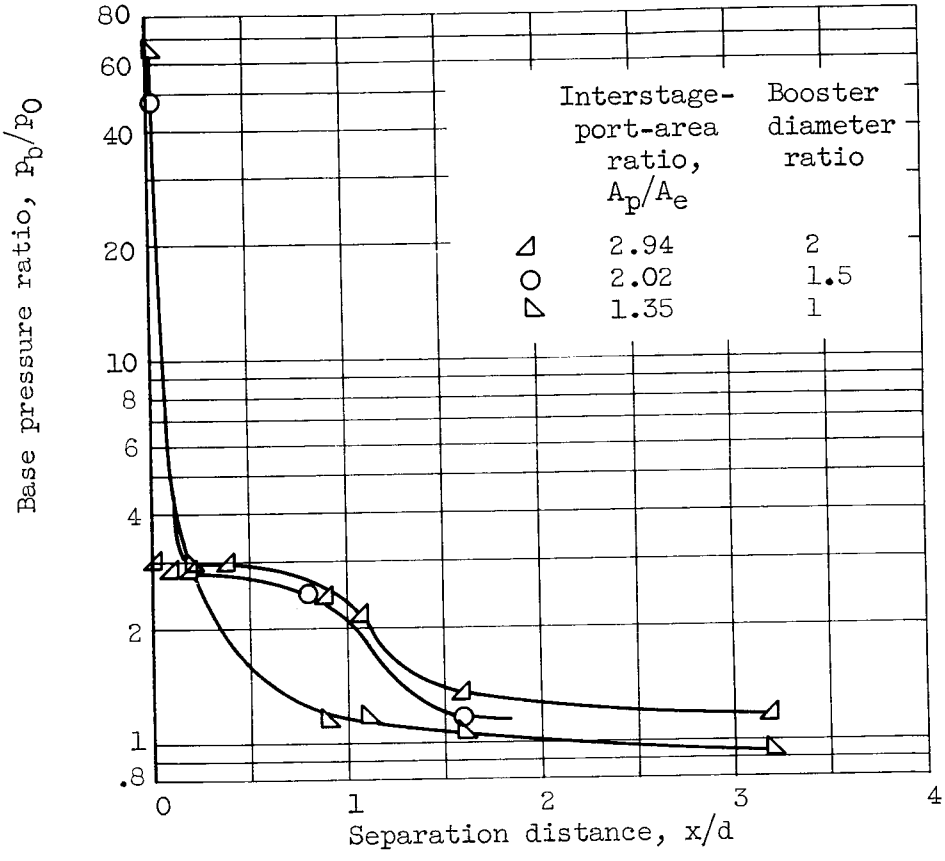

(b) Jet-on staging. Chamber pressure, 600 pounds per square inch absolute.

Figure 9. - Effect of booster diameter on upper-stage base pressure (12-port interstage).

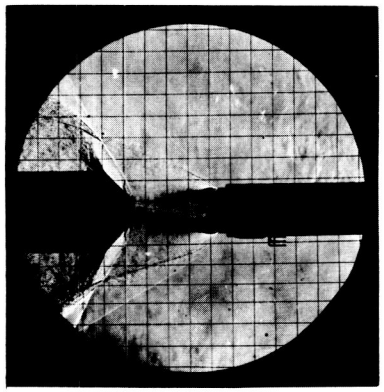

(a) Truncated isentropic nozzle. Separation distance, x/d = 1.6.

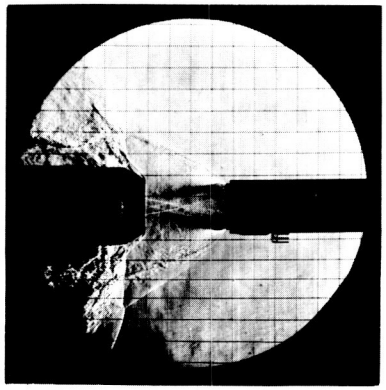

(b) Bell nozzle. Separation distance, x/d = 1.6.

C-61005

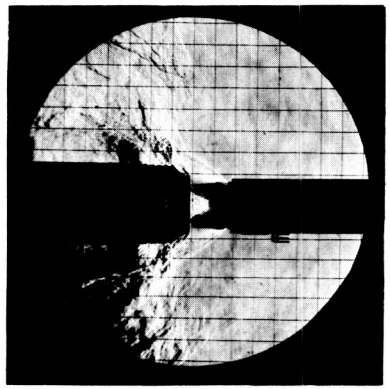

(c) Bell nozzle. Separation distance, x/d = 0.8.

Figure 10. - Nozzle flow patterns.

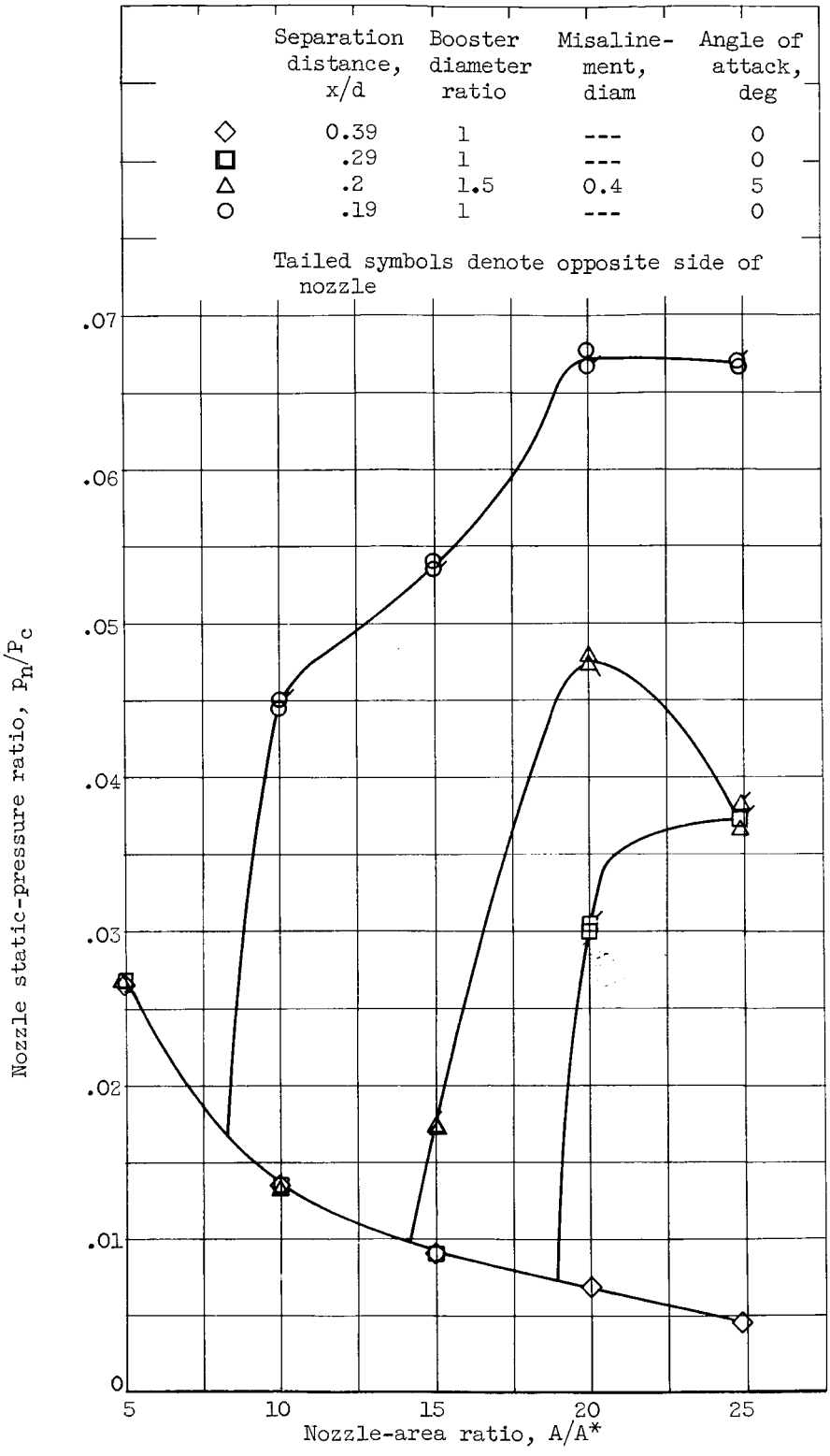

Figure 11. - Nozzle-pressure distributions.

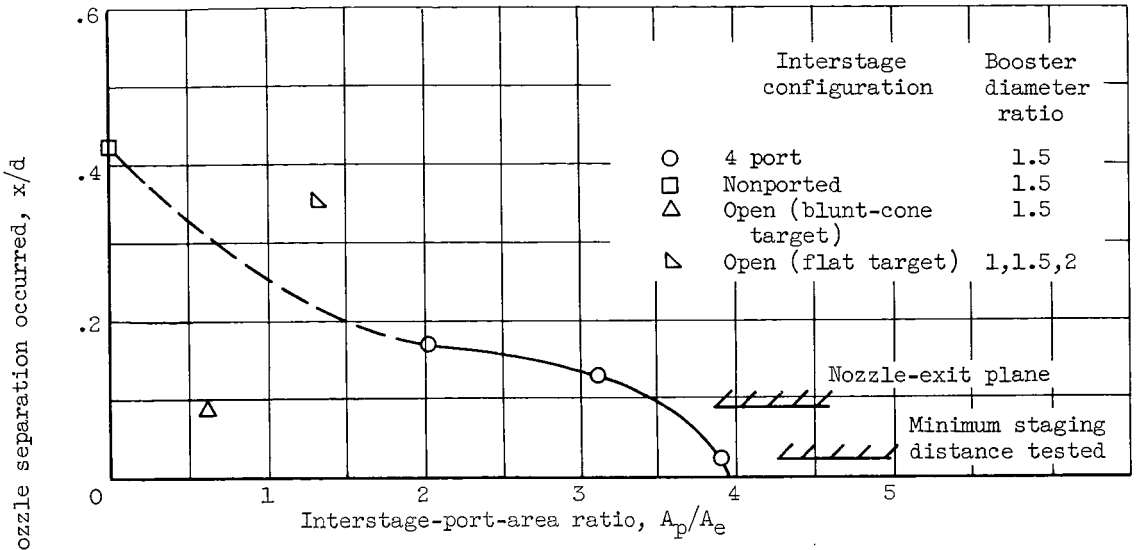

(a) Variation of interstage-port area.

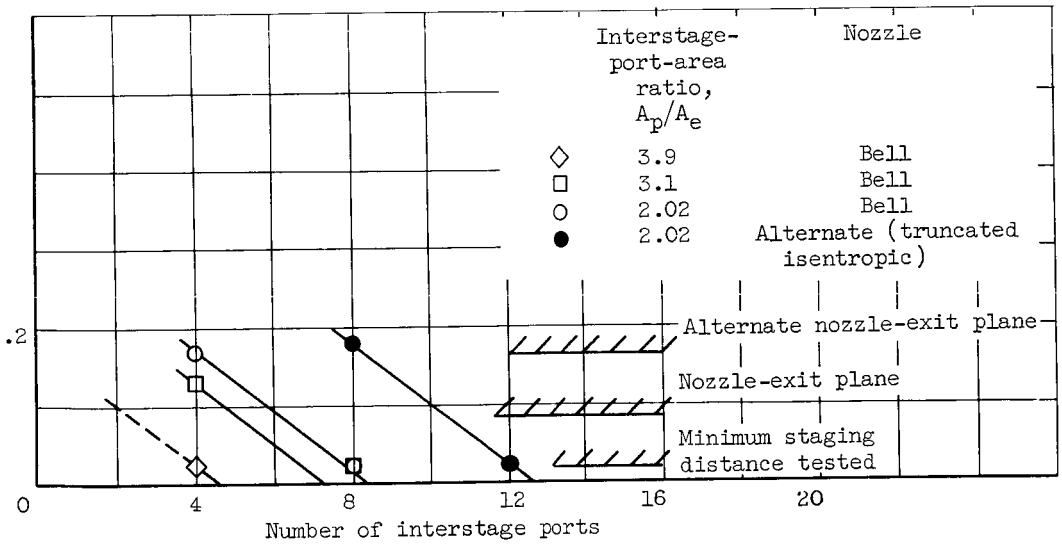

(b) Variation of number of interstage ports; 1.5-diameter-ratio booster.

Figure 12. - Effect of interstage configuration on nozzle separation.

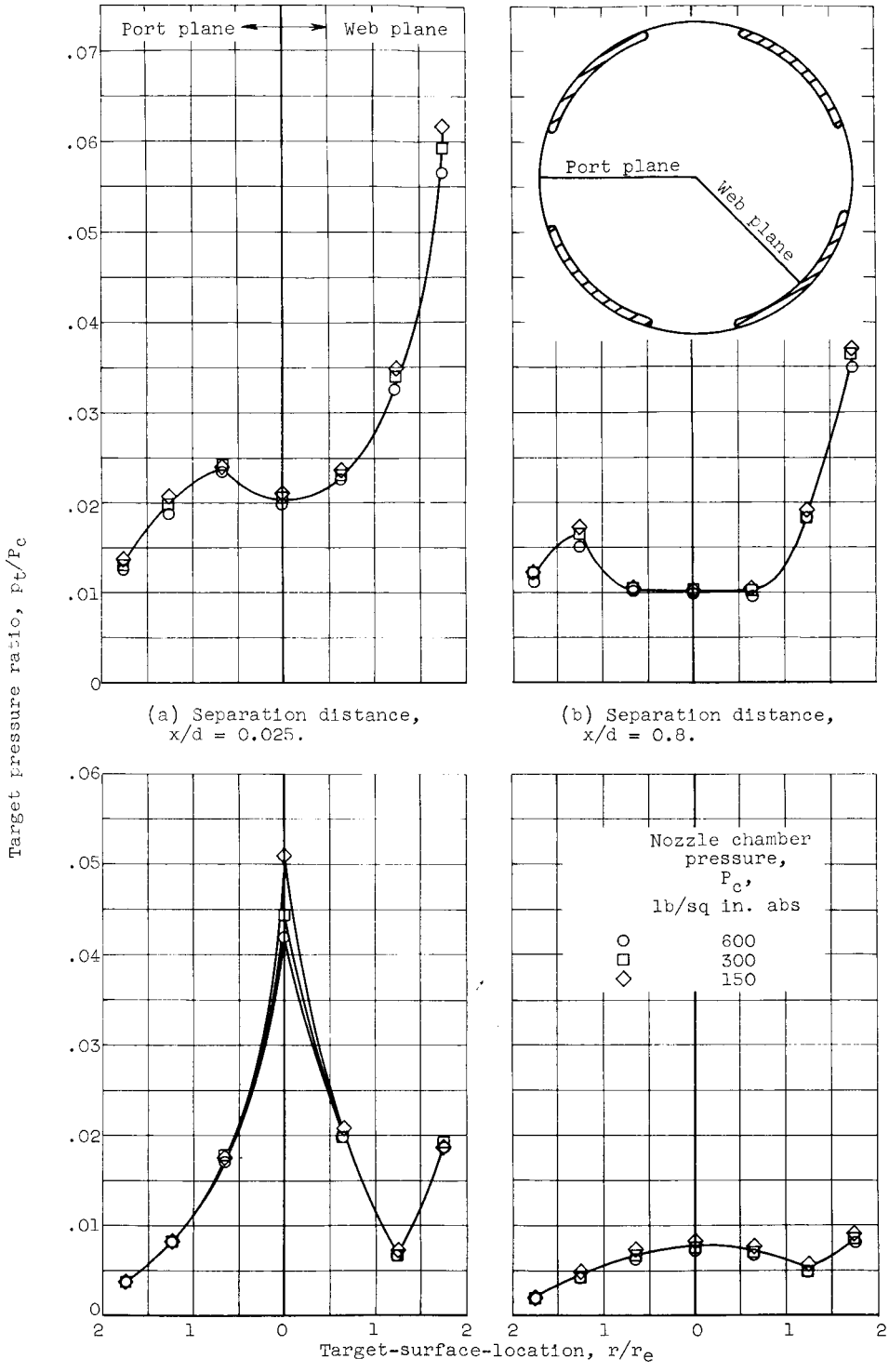

(a) Separation distance, x/d = 0.025.

(b) Separation distance, x/d = 0.8.

(c) Separation distance, x/d = 1.6.

(d) Separation distance, x/d = 3.2

Figure 13. - Pressure profiles on blunt-cone target within interstage configuration. 1.5-Diameter-ratio booster; number of interstage ports, 4; interstage-port-area ratio, 2.02.

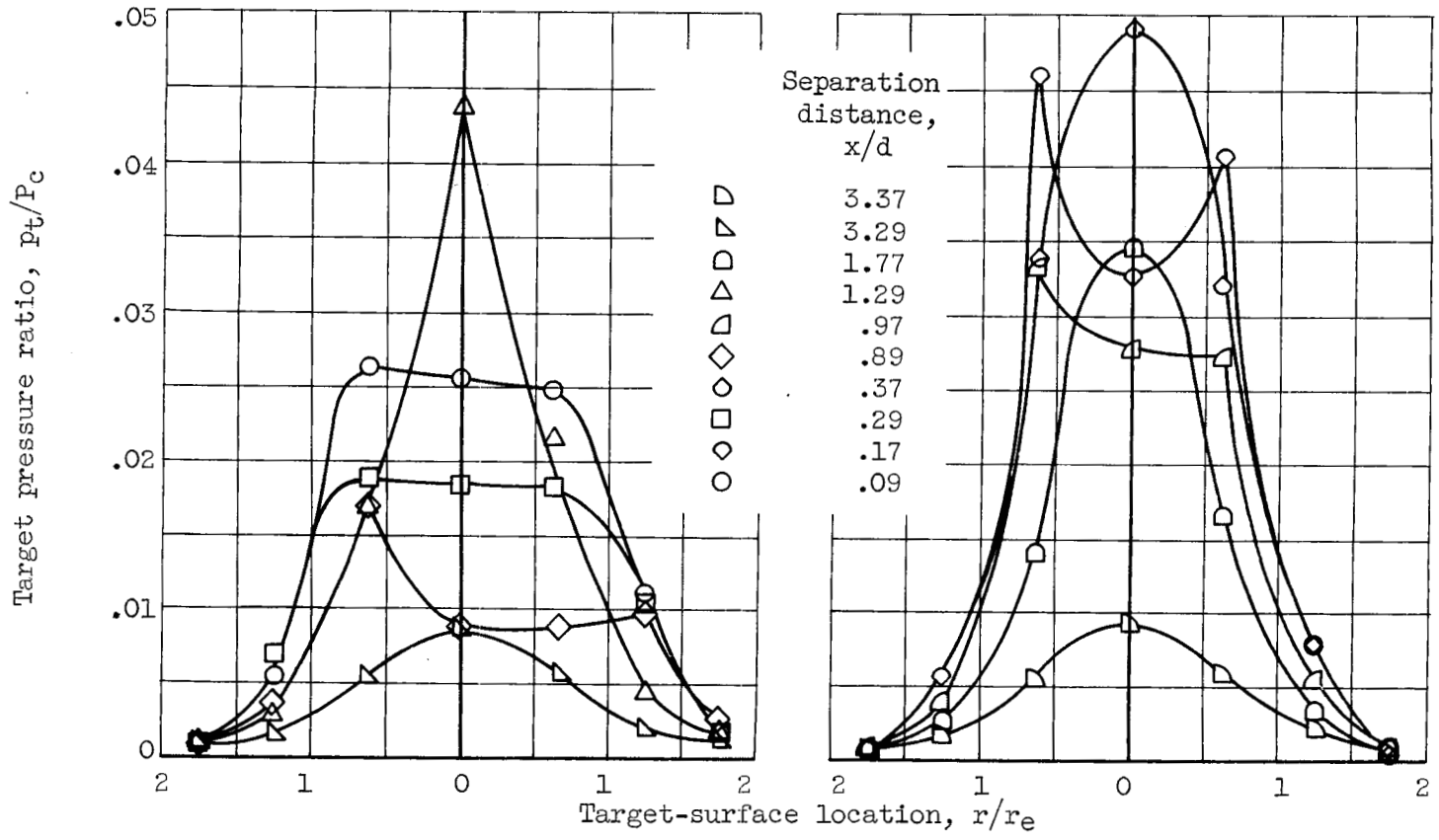

(a) Bell nozzle.

(b) Truncated isentropic nozzle.

Figure 14. - Pressure profiles on blunt-cone targets. 1.5-Diameter-ratio booster with open interstage.

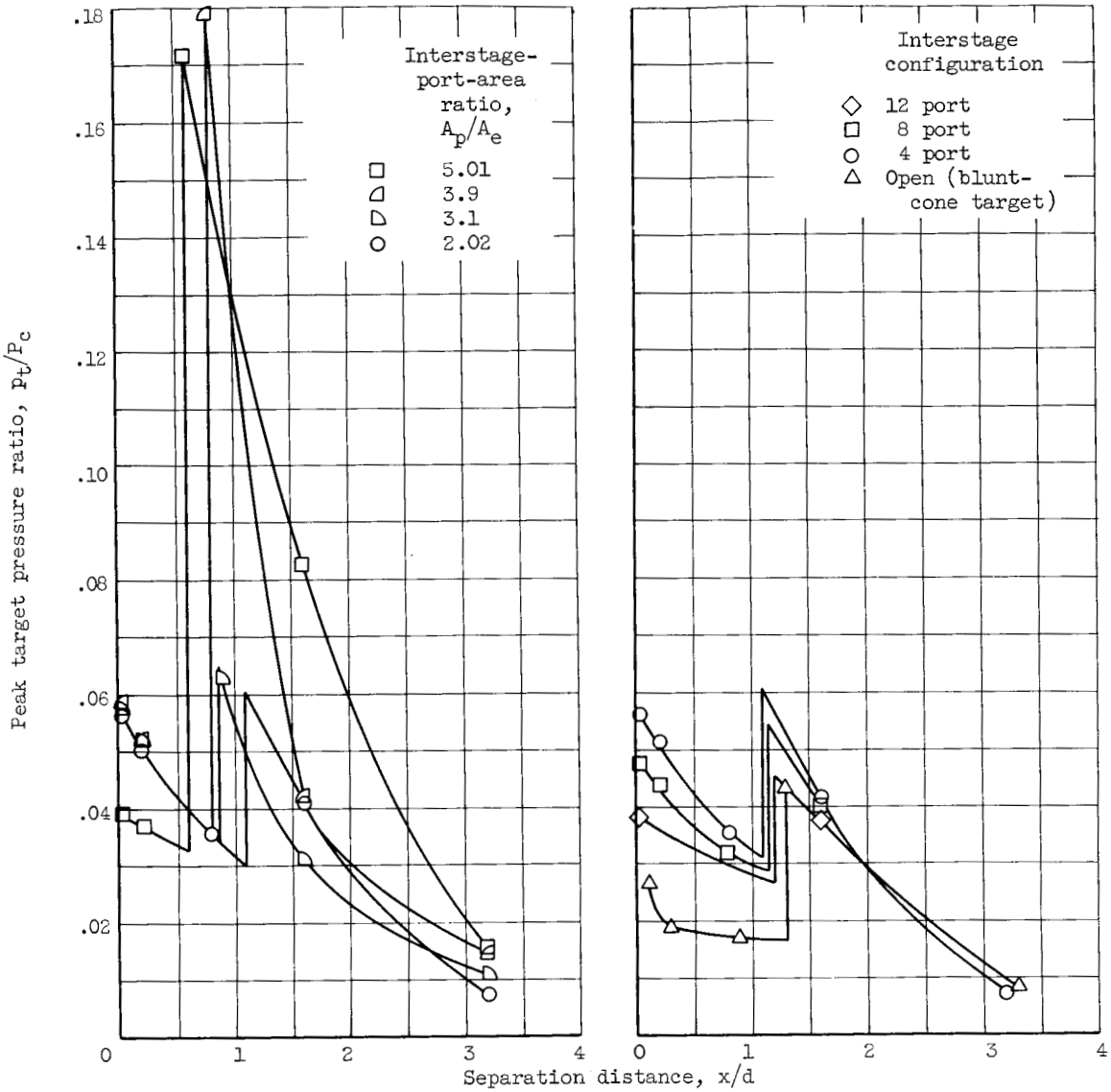

(a) Variation of interstage-port area. Number of interstage ports, 4.

(b) Variation of number of interstage ports. Interstage-port-area ratio, 2.02.

Figure 15. - Effect of interstage configuration on peak target pressures. 1.5-Diameter-ratio booster; chamber pressure, 600 pounds per square inch absolute.

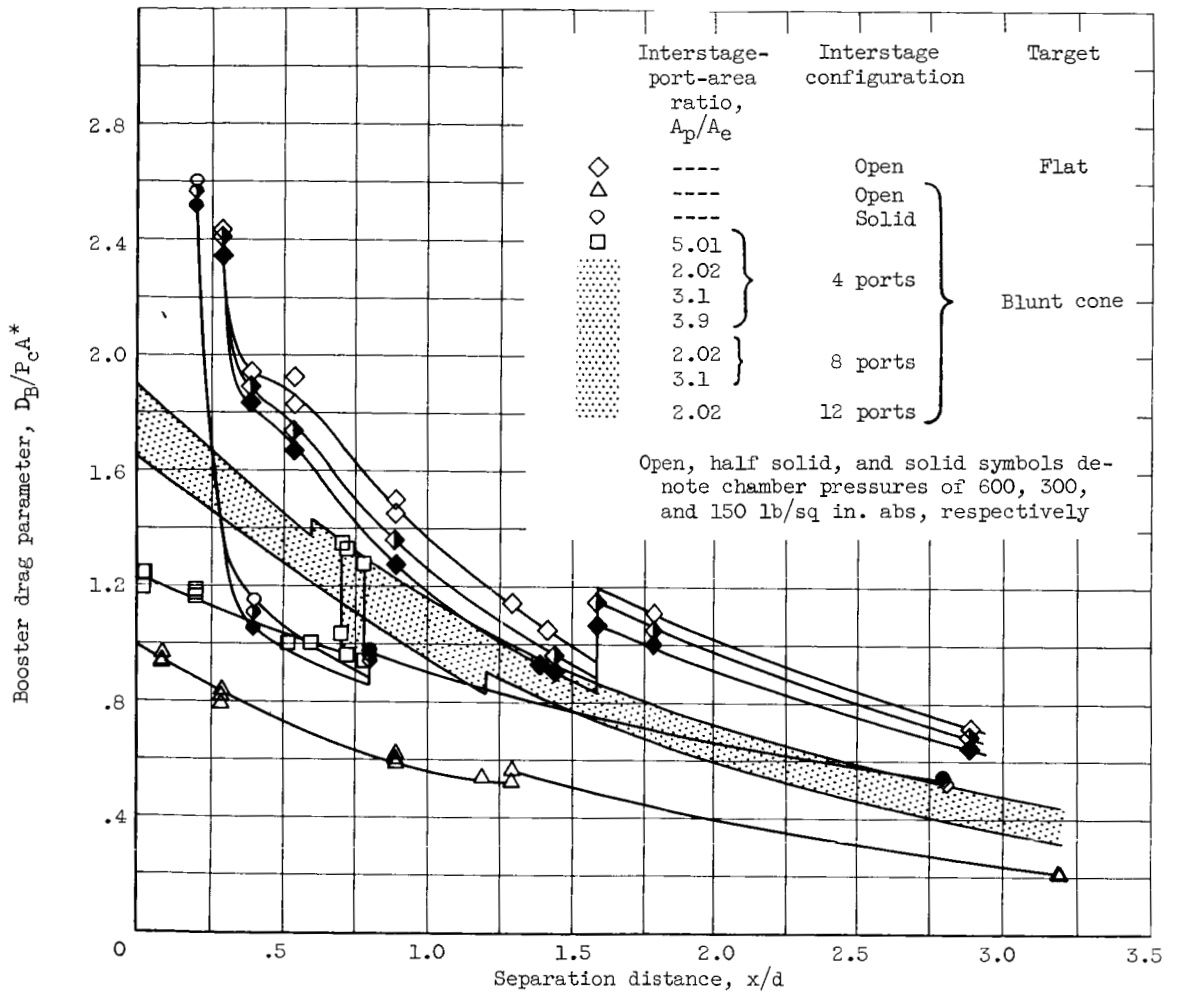

(a) 1.5-Diameter-ratio booster.

Figure 16. - Booster drag.

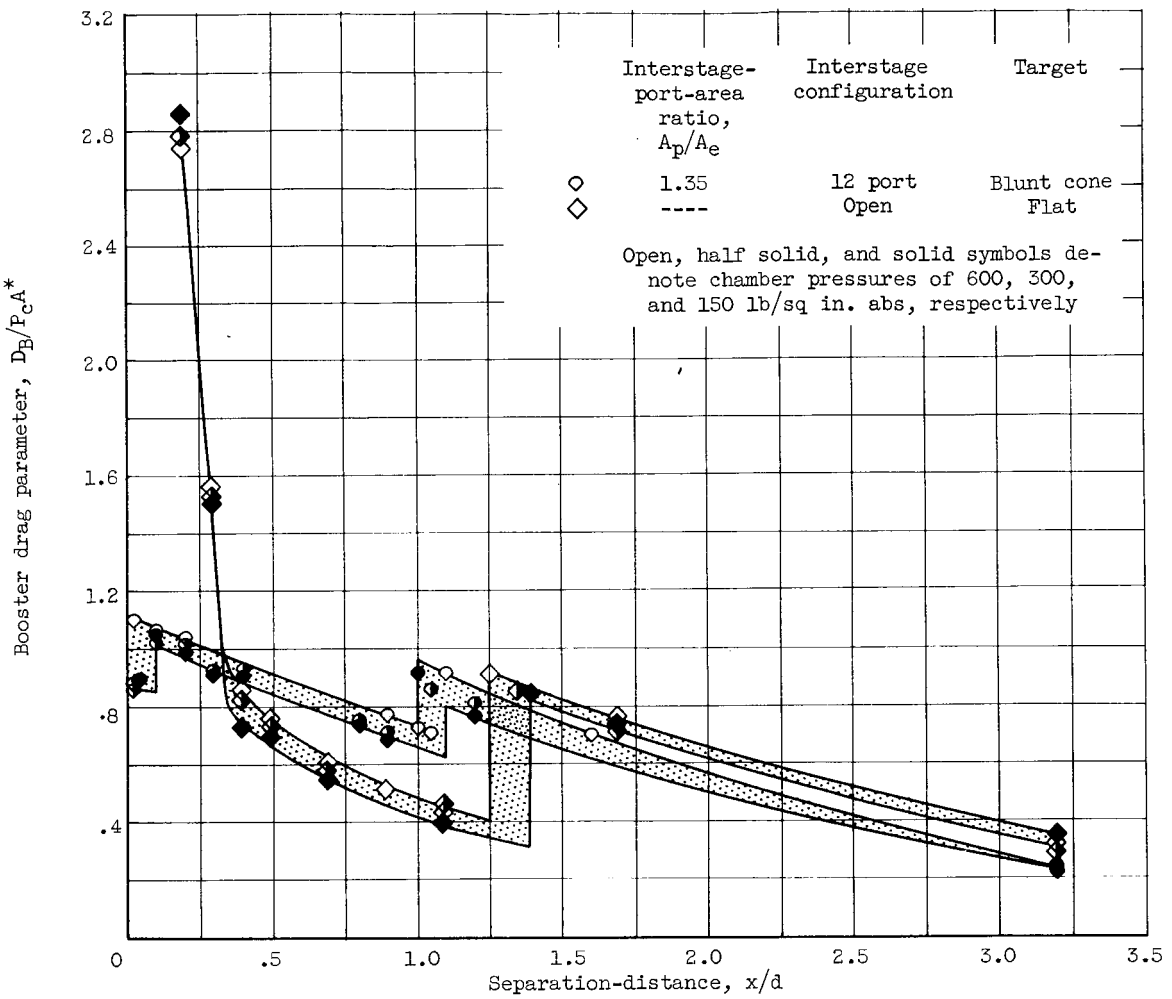

(b) 1-Diameter-ratio booster.

Figure 16. - Continued. Booster drag.

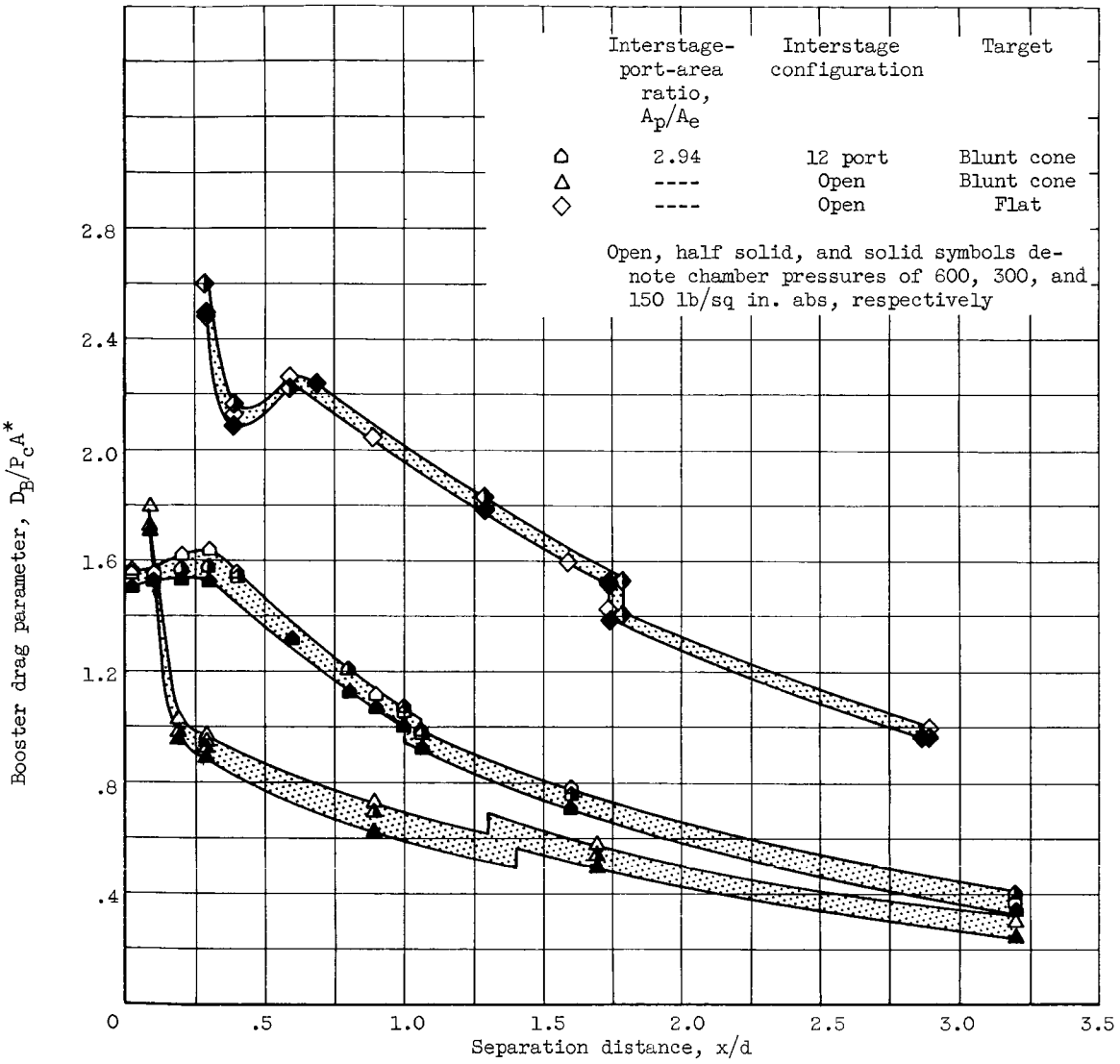

(c) 2-Diameter-ratio booster.

Figure 16. - Concluded. Booster drag.

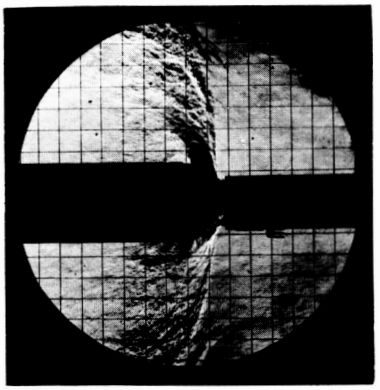

(a) Blunt-cone target. Separation distance, x/d = 0.09.

C-61006

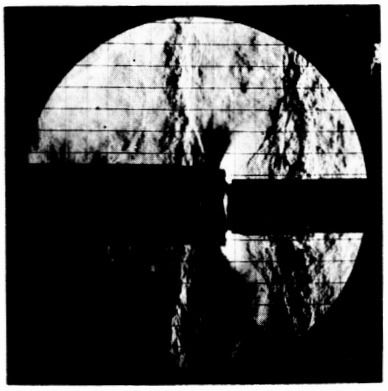

(b) Flat target. Separation distance, x/d = 0.29.

Figure 17. - Schlieren photographs of jet impingement on 1.5 diameter-ratio booster, open-interstage configurations.

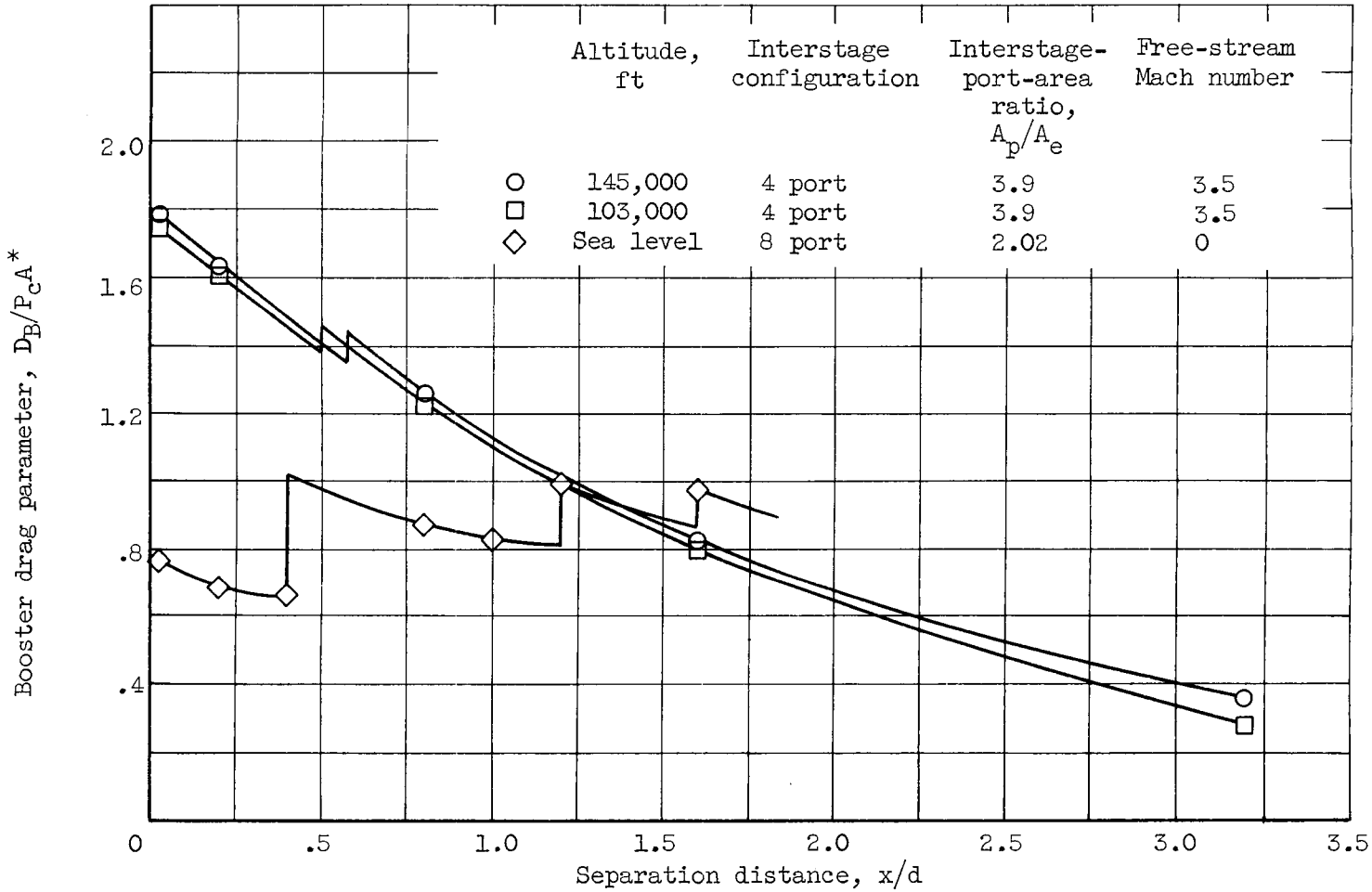

Figure 18. - Effect of altitude on booster drag. 1.5-Diameter-ratio booster; chamber pressure, 600 pounds per square inch absolute.

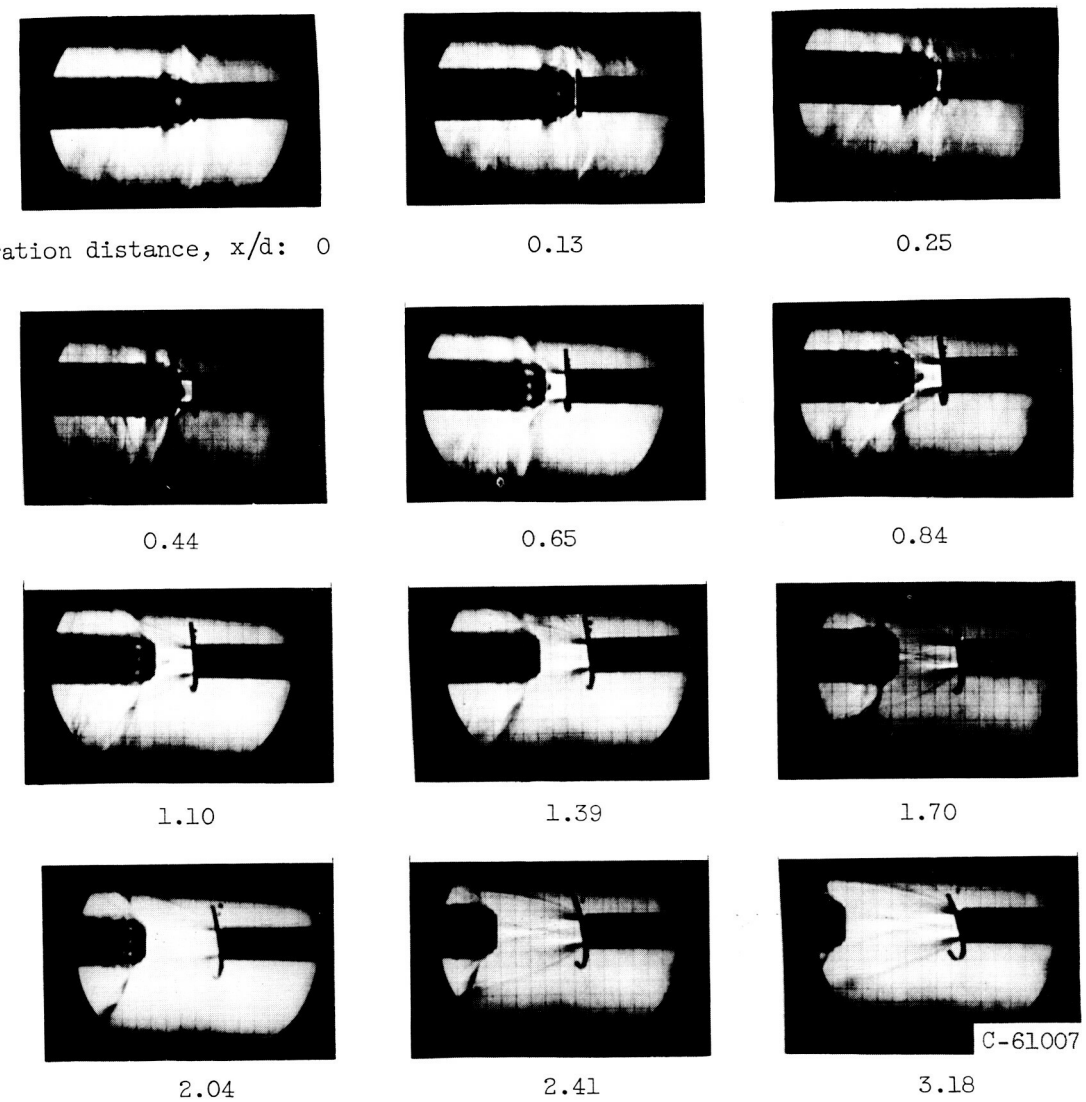

Figure 19. - Separation of 1.5-diameter-ratio booster. Chamber pressure, 600 pounds per square inch absolute.

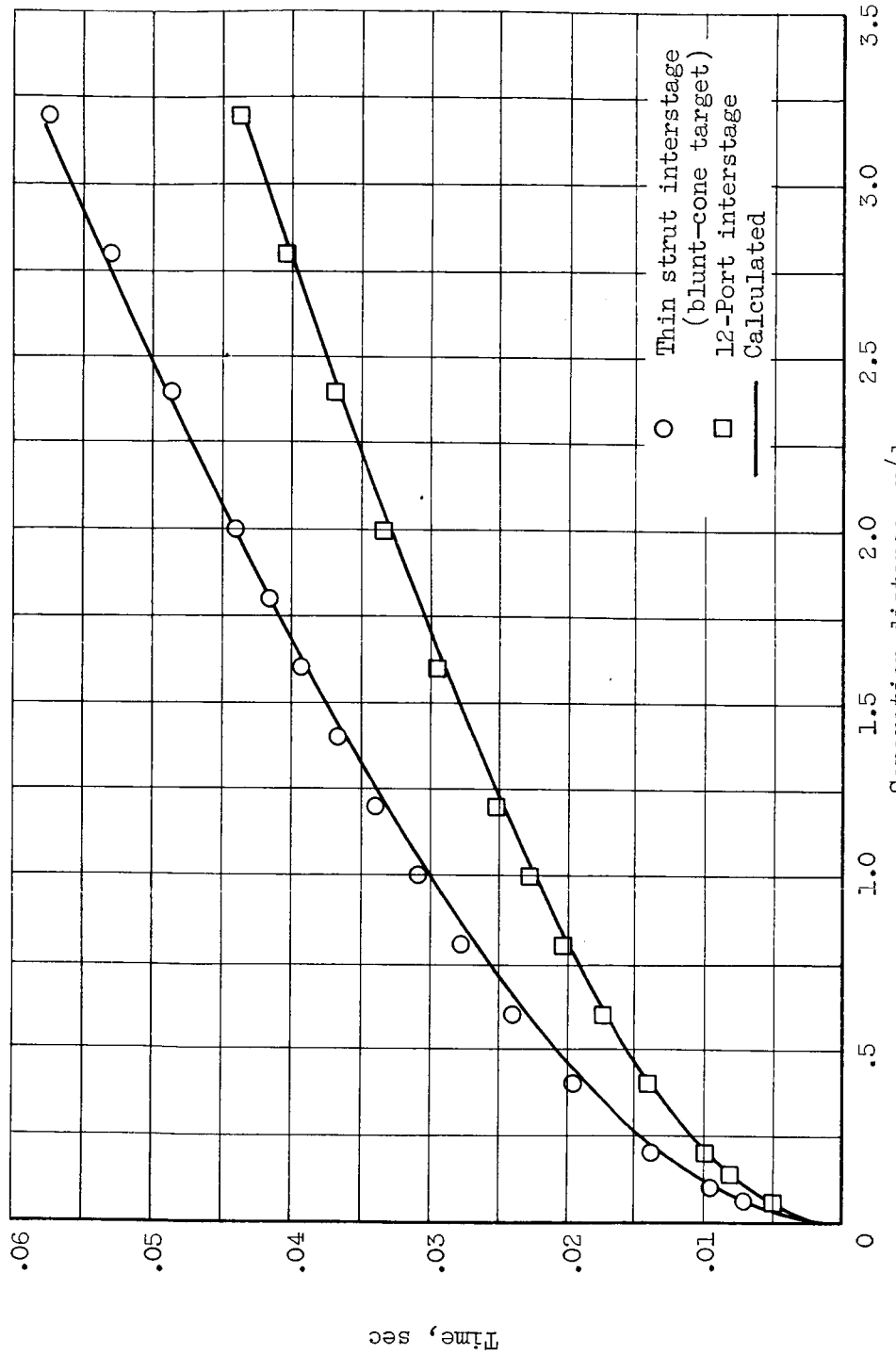

Figure 20. - Separation time for two 1.5-diameter-ratio boosters.